4. Spectral Measurements and Data Analysis

This chapter describes the spectral measurements routinely performed by the network instruments and the methods to process final data from the instrument's raw data. The method by which the irradiance calibration of standard lamps is transferred to solar data is described in detail, followed by a description of wavelength calibration methods and the way dose-rates and daily doses are calculated from spectral data. The procedure of calibrating data from GUV multi-channel filter radiometers is laid out in Section 4.3.

4.1. Types of Spectral Measurements of SUV-100 and SUV-150B Spectroradiometers

There are four types of instrument scans routinely performed by SUV-100 and SUV-150B spectroradiometers: Data, Response, Wavelength, and Absolute scans. An overview is provided in Tables 4.1 (SUV-100) and 4.2 (SUV-150B). *Data* scans measure solar irradiance while the rest are used for calibrations and quality control. *Response* scans determine system responsivity using the internal 45-Watt tungsten-halogen lamp as a source. *Wavelength* scans measure the positions of lines from the internal mercury discharge lamp. Results are used for the instrument's wavelength calibration and to determine the spectral bandwidth of the monochromator. *Absolute* scans are performed to calibrate the system using external 200-Watt tungsten-halogen standards of spectral irradiance. Additional scans are performed during special events like intercomparison campaigns or site visits. All scans are described in more detail in the following sections. Throughout spectral scans, measurements of auxiliary sensors (see Tables 2.1. and 2.2) are logged at varying intervals. The number of scans per day and the number of wavelengths measured per spectrum was historically a compromise between scientific needs and the challenge of transmitting large blocks of data from remote locations. See previous network operation reports for a description of historic modes of operation.

Table 4.1. Spectral scans performed by SUV-100 spectroradiometers, 2006 revision.

Scan	Wavelength increment	Range	Approx. Duration (hh:mm:ss)	Approximate File Size	Interval
Data Item 1	0.2 nm	280 to 345 nm	00:04:28		
Data Item 2	0.5 nm	335 to 405 nm	00:01:56		
Data Item 3	1.0 nm	395 to 605 nm	00:03:04		
Data Item 4	0.5 nm	280 to 290 nm	00:00:17		
Total Data			13 min	7 Kbytes	15 min during day light
Response	1.0 nm	280-605	00:05:06 per item (1 to 6 per day) plus 5 min. lamp warm-up	Up to 20 Kbytes	1 per day
Wavelength	0.1 nm	Segmented	16 min.	15 Kbytes	1 per day
Absolute	1.0 nm	250 to 700 nm	1 hour plus set-up time	20 Kbytes	Biweekly

Table 4.2. Spectral scans performed by SUV-150B spectroradiometer, 2006 revision.

Scan	Wavelength increment	Range	Approx. Duration (hh:mm:ss)	Interval
Data Item 1	0.2 nm	280 to 310 nm	00:04:13	
Data Item 2	0.2 nm	310.2 to 345 nm	00:01:56	
Data Item 3	0.5 nm	345.5 to 404 nm	00:02:33	
Data Item 4	0.5 nm	404.5 to 605 nm	00:04:31	
Total Data			00:14:09	15 min during day light
Response	1.0 nm	250-700	00:45:00 (3 items plus 10 min. lamp warm-up)	1 per day
Wavelength	0.1 nm	Segmented	00:30:00	1 per day
Absolute	1.0 nm	250 to 700 nm	1 hour plus set-up time	Biweekly

4.1.1. Data Scan

Data scans measure through-monochromator PMT-current caused by solar radiation. Whenever the Sun is above the horizon, they are performed every 15 minutes, indexed at the top of the hour.

4.1.1.1. SUV-100 Data Scan

Data scans from SUV-100 spectroradiometers are divided into four separate scan segments, called "items," to allow measurements with different instrument sensitivity (i.e., different settings of the PMT high voltage) in different spectral regions. At short wavelengths (280-345 nm), the highest sensitivity (or highest PMT voltage) is applied. If this sensitivity were maintained beyond 345 nm, the instrument would saturate. Therefore, a smaller PMT voltage is applied for longer wavelengths (Items 2 and 3). A typical SUV-100 data scan is shown in Figure 4.1. Between 280 and 345 nm, solar data is sampled in 0.2 nm steps (Item 1); between 335 and 405 nm the wavelength increment is 0.5 nm (Item 2). Item 3 is sampled in 1.0 nm steps between 395 to 605 nm and includes most of the Photosynthetically Active Radiation (PAR) or "visible" portion of the spectrum. Wavelengths between 335 and 345 nm and these between 395 and 405 nm are measured by two different items. When items overlap, the lower item data are published.

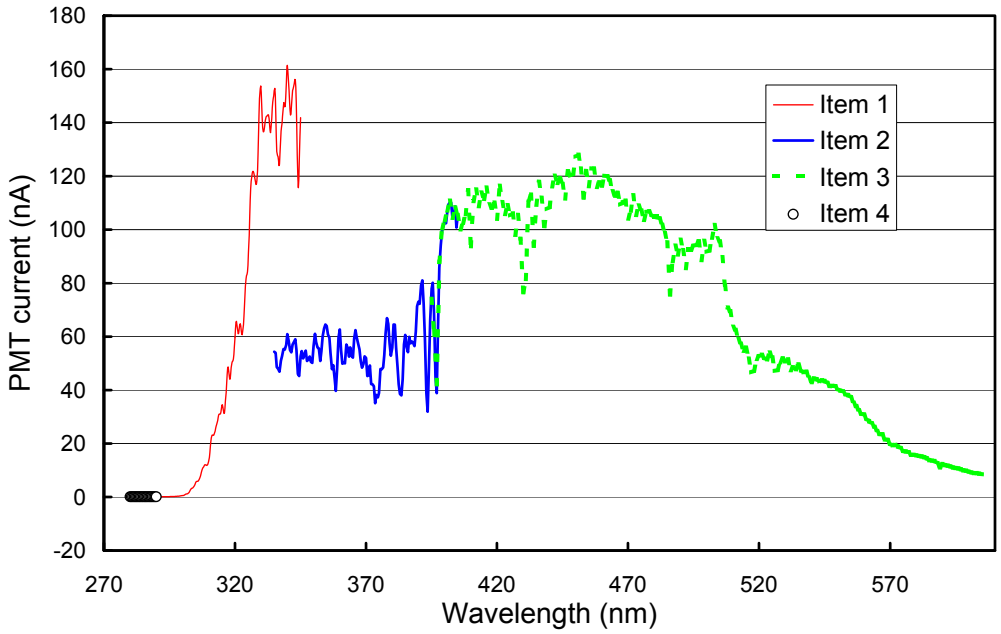

Figure 4.1. *SUV-100 Data Scan: PMT current during solar measurements before conversion to irradiance. Item 1 covers the spectral range 280-345 nm; Item 2 335-405 nm; and Item 3 395 to 605 nm. Item 1 is measured with a higher PMT voltage than Items 2 and 3. Item 4 (280-290 nm) is a measurement of the PMT dark current with the same PMT voltage applied as during Items 2 and 3.*

In the course of data evaluation, the PMT dark current (i.e., the PMT current without radiation falling on the PMT's photo-cathode) is subtracted from the measurements (see Section 4.2.1.2.). Since there is no detectable solar radiation impinging the Earth's surface with wavelength below 290 nm, the dark current assigned to Item 1 is simply the average of measurements between 280-290 nm, calculated from the same segment. A data scan also includes a fourth item; a scan from 290 to 280 nm in steps of 0.5 nm, carried out with the same PMT high-voltage setting as for the Items 2 and 3. Since the PMT dark currents are measured with the shutter open, stray light (e.g., photons with wavelengths above 290 nm that are registered at wavelengths below 290 nm) may also fall on the PMT cathode. Systematic errors in the measurement due to stray light (if present), are partly reduced when subtracting the dark current.

At the beginning of Item 1 and Item 2, a delay of about 1-minute is specified to allow the PMT to stabilize at the new high voltage setting. A typical data scan takes about 13 minutes to complete. Figure 4.2 shows the approximate relationship between time and wavelength. This function may slightly change from scan to scan, and is also slightly different for each site. The start time of Item 1 is listed for each data scan in the field "TimeA" of the published Database 1. Similarly, the start of Item 2 is given in the field "TimeB" of Database 2. Start time of item 1 and end time of item 3 are also given in the header of composite scans.

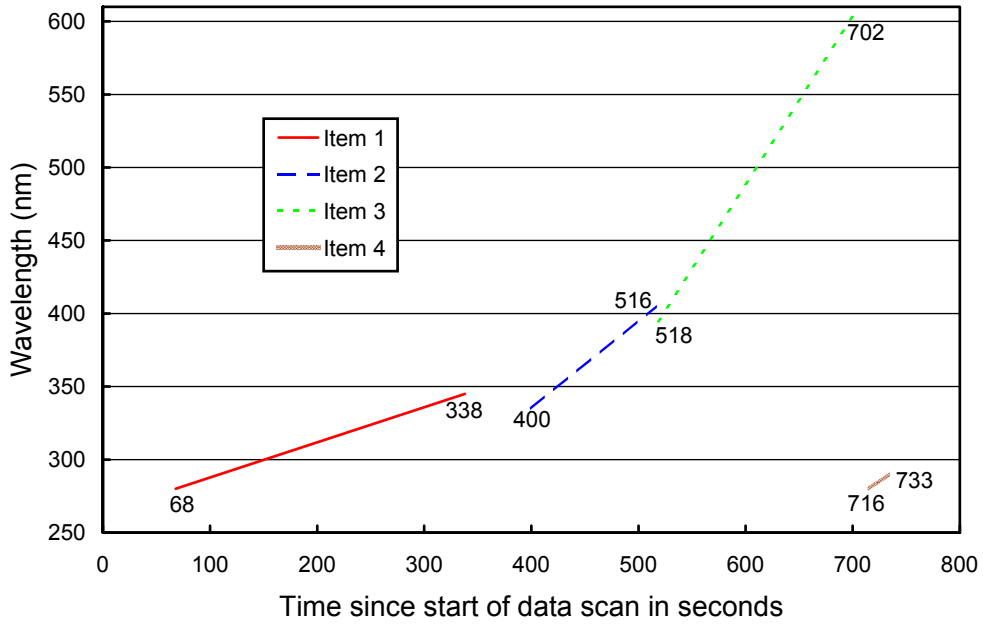

Figure 4.2. *Relationship of "time since start of a data scan" and wavelength, measured by all four items of a data scan. Data are from the instrument in San Diego. The numbers are start and end times of the different items in seconds. Note that item 4 goes from 290 to280 nm rather than from 280 to 290 nm.*

The PMT high voltage setting of data scans is diurnally optimized to produce a maximum dynamic range without overload. These automatic adjustments can result in the use of one to six different PMT high-voltage regimes per day, depending on time-of-year and location. Spectral irradiance values, calculated from the data scan, are displayed in Figure 4.3 (linear y-axis) and Figure 4.4 (logarithmic y-axis).

Since the start of network operation in 1988, several changes have been made to the data scan. The item 2 segment upper limit was increased first from 350 nm to 380 nm (1994-95), and again to 405 nm (1996) to further increase scan-resolution of the UV-A to visible band. These extensions required reductions in sensitivity to avoid saturation. The slight loss of sensitivity when the segment was extended up to 405 nm in 1996 was partly compensated for by introduction of a new feature into the SUV-100 System Control Software that allows diurnal changes in PMT high voltage as a function of solar zenith angle (SZA). This resulted in maintenance of an optimum sensitivity throughout the day. The terminal wavelength for the item 3 scan was also reduced from 700 to 620 nm (1994-95) and again to 605 nm (1996). The system sensitivity at wavelengths longer than 600 nm is poor due to the monochromator and PMT optimization for the ultraviolet. In examining the data, we found that this sensitivity was so poor that we advise users to ignore data beyond 600 nm. A change to the wavelength increment of the Item 3 segment was in response to requests of data users. In the 1991-1992 season, the increment was changed from 5 nm to 2.5 nm, and during the 1992-1993 season, it was further reduced to 1 nm.

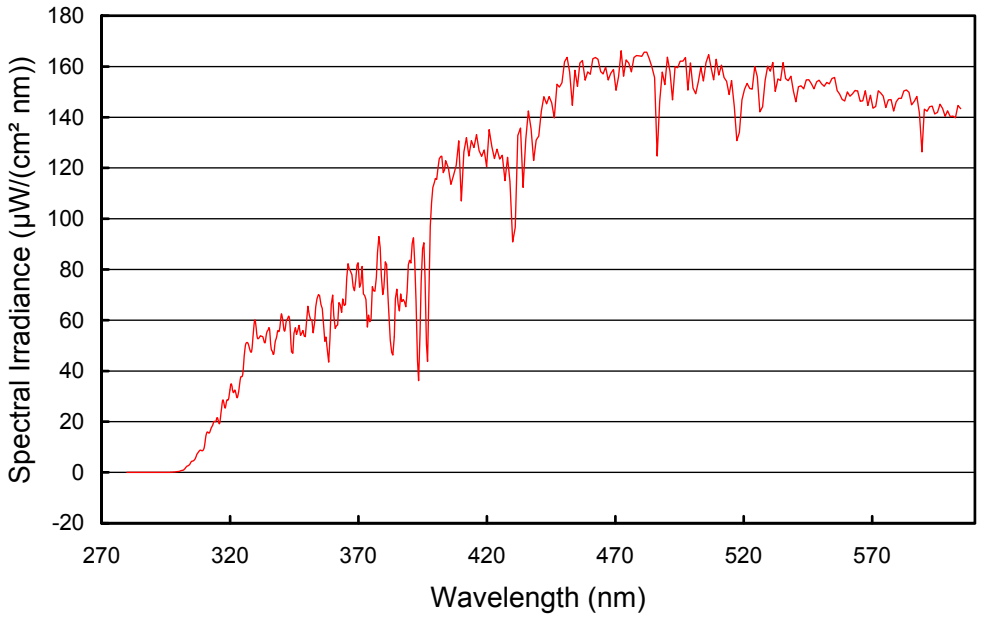

Figure 4.3. *Irradiance calculated from the PMT currents shown in Figure 4.1. Data from Items 1-3 are included.*

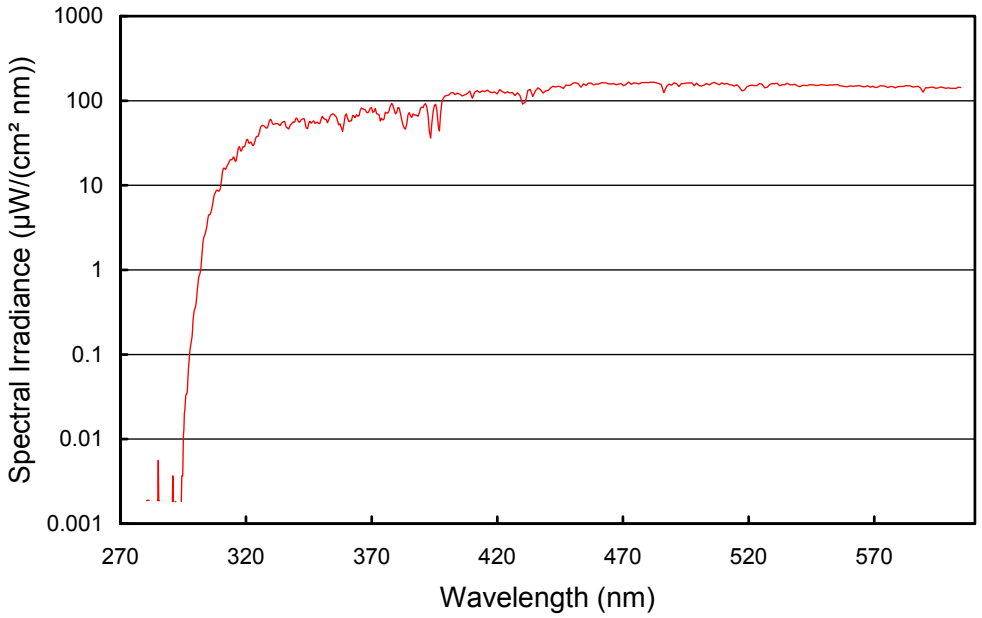

Figure 4.4. *Same as previous figure but presented on logarithmic y-axis to demonstrate the steep decline of the solar spectrum in the UV-B. The spikes between 280 and 290 nm indicate the detection limit of the instrument, which is caused by signal noise.*

4.1.1.2. SUV-150B Data Scan

Data scans from the SUV-150B spectroradiometer at Summit are also divided into four items. The PMT high voltage is identical for all items, but integration time and wavelength increment vary. Item 1 is sampled in 0.2-nm steps from 280 to 310 nm, applying an integration time of 1.3 seconds. Wavelength range, wavelength increment, and integration times for items 2-4 are as follows: Item 2: 310.2–345 nm, 0.2 nm, 0.5 s; Item 3: 345.5–404 nm, 0.5 nm, 0.5 s; Item 4: 404.5–605 nm, 0.5 nm, 0.17 s. A typical SUV-150B data scan is shown in Figure 4.5. The PMT dark current is calculated from measurements between 280 and 290 nm.

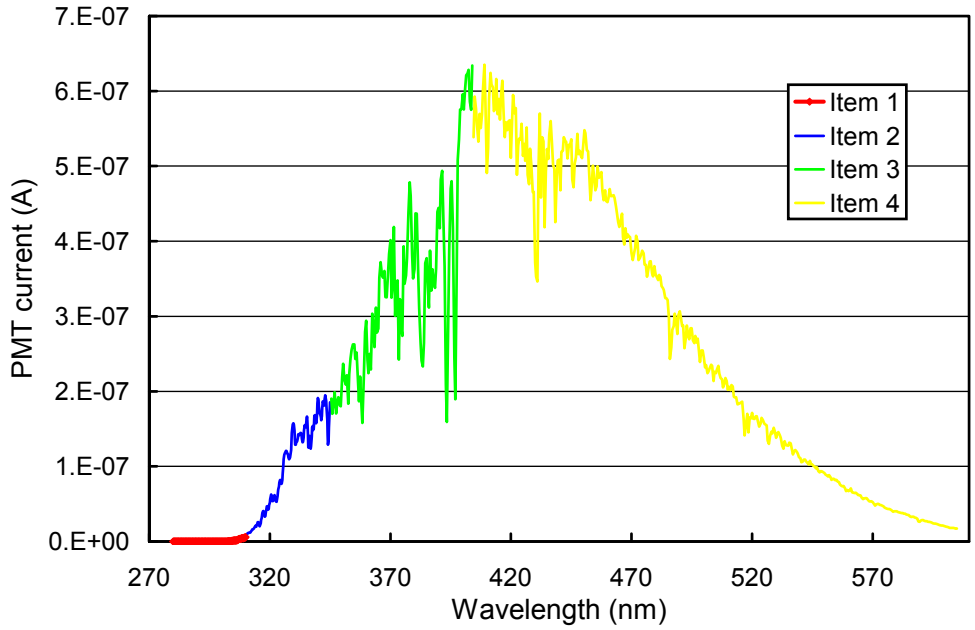

Figure 4.5. *SUV-150B Data Scan: PMT current during solar measurements before conversion to irradiance. Item 1 covers the spectral range 280-310 nm; Item: 2 310.2-345 nm; Item 3: 345.5-404 nm; and Item 4: 404.5-605 nm*

A typical data scan takes about 14 minutes to complete. Figure 4.6 shows the approximate relationship between time and wavelength. The start time of each data scan is listed in the field "TimeA" of the published Database 1. The start times of Item 3 is given in Database 2. Composite scans provide times at each wavelength.

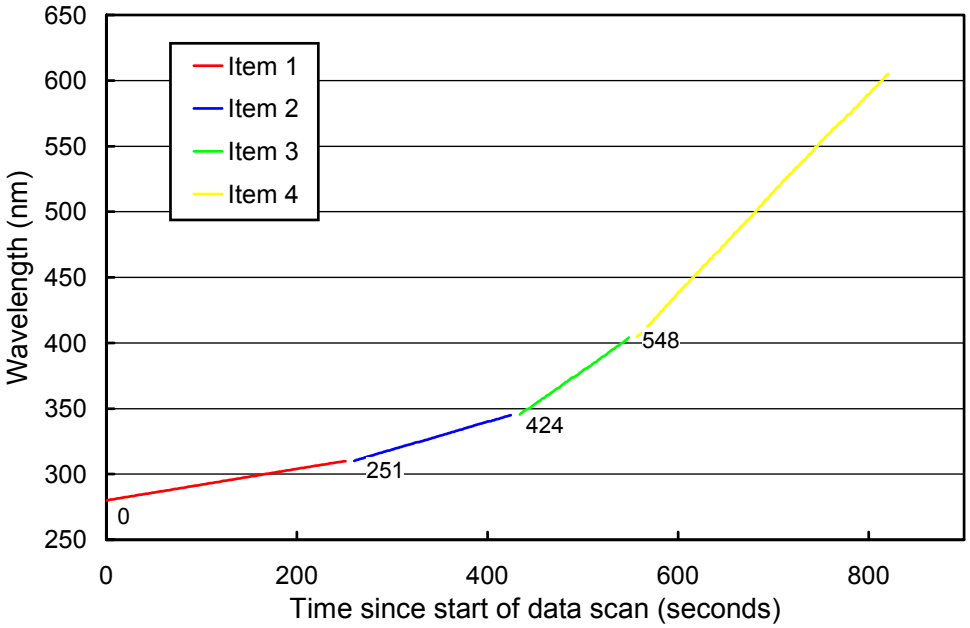

Figure 4.6. *Relationship of "time since start of a data scan" and wavelength, measured by all four items of a SUV-150B data scan. The numbers are start times of the different items in seconds.*

4.1.2. Response Scan

Response scans measure the PMT current when the internal 45-Watt tungsten-halogen lamp of a SUV spectroradiometer is energized. These scans are typically performed once per day. Response scans track changes in system responsivity and are used for adjustment of the instrument's calibration. As described above, PMT high voltages applied during SUV-100 data scans depend on solar zenith angle. A response scan consists of several items with different PMT high voltages applied, which match the voltages used during that day's data scans. Prior to initiating the scan segments, an adequate lamp stabilization period following power-up ensures that the lamp reaches thermal equilibrium before the scan. After the "warm-up" period, the lamp drive current is then adjusted to a target setting and accurately controlled (Section 2.5). Figure 4.7 shows typical data recorded from a SUV-100 response scan. The lines represent PMT currents as a function of wavelength for a six-item response scan, at the various sensitivities (PMT high voltages) used in a single diurnal cycle. For quality control purposes, TSI sensor readings and the response lamp drive current are also recorded during the response scan. These parameters are reviewed to ensure that there are no response lamp changes during these scans.

Data scans of the SUV-150B use only one high voltage setting. SUV-150B response scans consist of three items. Items 1 and 2 are measured with the same high voltage as data scans. Item 3 is a "dark" measurement with the lamp switched off.

4.1.3. Internal Wavelength Scan

Wavelength scans with the built-in mercury lamp are performed to align the wavelength position of the system to the actual wavelength of photons passing the monochromator. In addition, wavelength scans allow identifying changes in the bandpass (or bandwidth) of the monochromator. Usually one wavelength scan per day is scheduled. The wavelength scan is composed of a series of segments, with the shutter closed and internal mercury discharge lamp energized. Segments are chosen to concentrate high spectral resolution scanning in areas throughout the spectroradiometer's sensitive range, where significant mercury lines occur. The PMT high voltage settings for each segment are optimized to maximize the signal observed at the peaks of the mercury lines. A typical multiple-item scan of a SUV-100 spectroradiometer

is shown in Figure 4.8. Internal wavelength scans of the SUV-150B are similar, but have a smaller bandpath.

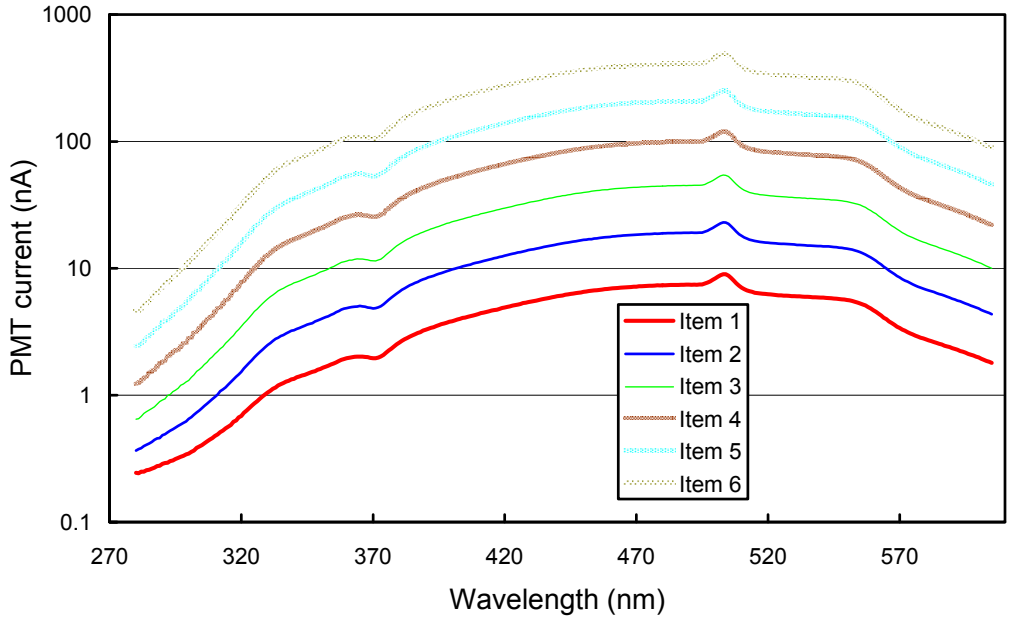

Figure 4.7. *Six-item SUV-100 response scan. Note that PMT dark current is not subtracted.*

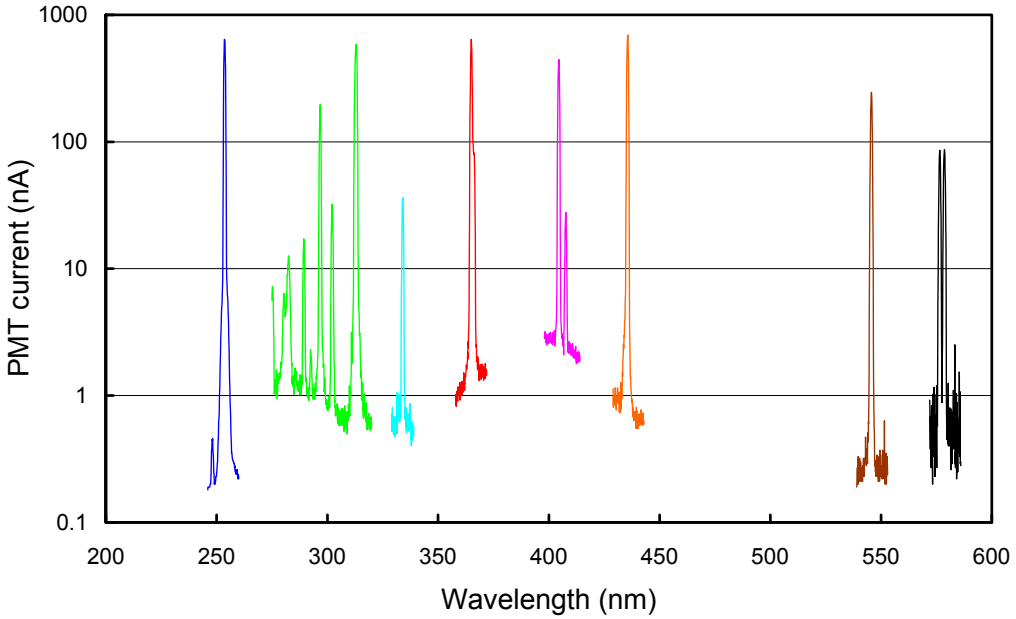

Figure 4.8. *Typical multi-peak wavelength scan with eight segments. In a typical wavelength scan, the baseline value may show variation across the spectrum due to fluorescence from the lamp. Note that PMT dark current has not been subtracted.*

4.1.4. External Wavelength Scan

We determined at the Boulder, Colorado 1994 intercomparison (Thompson et. al., 1997) that wavelength scans performed with internal and external sources differ due to different light paths for both scan types. Radiation from the internal mercury lamp passes through two beam-splitters and enters the monochromator's entrance slit without further scattering. Radiation from an external mercury lamp is scattered first by the cosine collector before it enters the monochromator. Due to the different light path geometries the monochromator's gratings are illuminated differently causing the deviation observed in the wavelength registration. The effect is more pronounced for SUV-100 instruments than for the SUV-150B. Beginning with the site visits of the 1994-1995 season, external wavelength scans have been performed as a routine part of the site visit. These scans provide a realistic measurement of the systems' bandpass and wavelength mapping, as the light path of external scans is the same as that for solar irradiance measurements.

During the external wavelength scan, a mercury lamp is placed on top of the collector such that it fills the entire field-of-view of the PTFE diffuser. The external wavelength scan is composed of a series of items that are spectrally identical to internal wavelength scan segments. A comparison of the 296.73 nm line measured by typical external and internal mercury scans of a SUV-100 is shown in Figure 4.9. The peaks of the external scans, which has the same light path as solar measurements, agree well with the nominal wavelength of 296.73 nm, whereas the peaks of the internal scans are shifted about 0.1 nm to shorter wavelengths. External scans have a bandwidth of about 1.0 nm FWHM at 296.73 nm. The bandwidth of external scans in the visible varies between 0.8 and 1.0 nm. The bandwidth of the internal scan is typically 0.75 nm. Until the release of Volume 6, no attempt was made to correct for these effects, i.e., the wavelength mapping was solely based on internal scans; external scans were only used for documentation. Starting with Volume 7, a different method for wavelength calibration was implemented, which is described in Section 4.2.2.2. As an example, Figure 4.9 shows measurements performed in 2001 and 2002 at Palmer Station. Data from the two years are very reproducible, demonstrating good stability of the system.

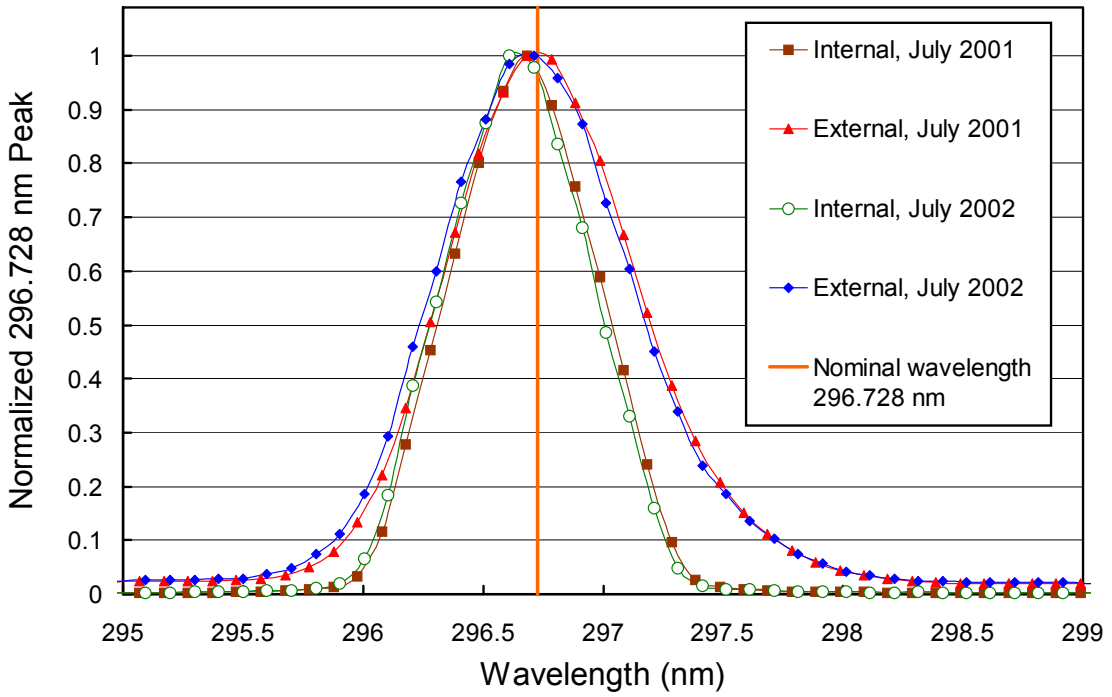

Figure 4.9. *Normalized mercury-line peaks from external and internal wavelength scans. Data is from the SUV-100 at Palmer Station. The comparison of data from 2001 and 2002 demonstrates the good stability of the system.*

4.1.5. Absolute Scan

The purpose of absolute scans is to transfer the irradiance scale from 200-Watt tungsten-halogen standards of spectral irradiance ("site standards") to the internal 45-Watt irradiance reference lamp. In addition, absolute scans are sometimes used to compare different 200-Watt standards, and to re-calibrate lamps. Under normal circumstances, when the system is stable and operating properly, these scans are performed biweekly. In order to perform an absolute scan, the 200-Watt lamp is positioned in a specially designed lamp stand outside the roof box such that the distance from the lamp filament to the diffuser of the SUV spectroradiometer collector is 50 cm, as specified in the calibration certificate of the 200-Watt lamp (see Section 2.5 for details).

4.1.5.1. Absolute scan SUV-100

Figure 4.10 shows a typical absolute scan of a SUV-100 spectroradiometer. This scan consists of eight segments, where the first four items characterize system behavior at short wavelengths (250-330 nm), and the last four segments characterize behavior between 250 nm and 700 nm. The reason for having two sets of four items is to optimize the system sensitivity via PMT high voltages for different parts of the spectrum. Items 1 through 4 are run at the same PMT high voltage setting, and 5 through 8 are run at a lower high voltage setting. Each of the two sets has the following segments:

- Items 1 and 5 are performed with the lamps turned off and the shutter open; it measures PMT dark current for the following 200-Watt lamp scan and detects any light leaks.
- Items 2 and 6 measure PMT current with the 200-Watt lamp on and the shutter open.
- Item 3 and 7 measure PMT current with the 45-Watt lamp on and the shutter closed.
- Item 4 and 8 measure PMT dark current with the lamps turned off and the shutter closed.

A warm-up time of 6 minutes is applied preceding measurements of both lamps.

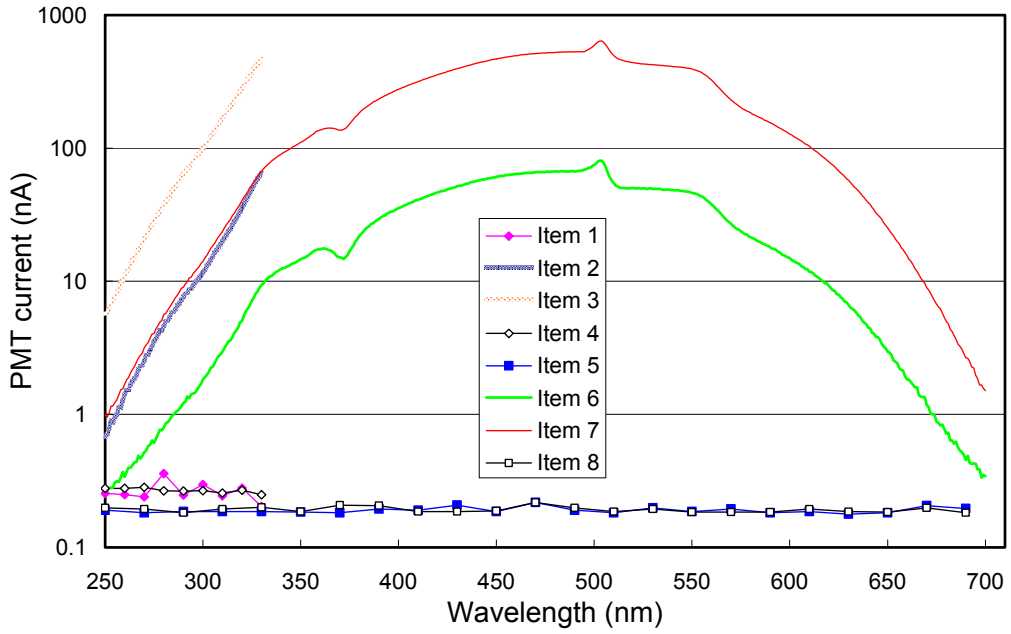

Figure 4.10. *Typical eight-item absolute scan of a SUV-100 spectroradiometer.*

4.1.5.2. Absolute scan SUV-150B

Figure 4.11 shows an absolute scan of the SUV-150B spectroradiometer. This scan consists of five items, which have identical wavelength settings but different integration times.

- Item 1 measures PMT dark current with the Instrument's shutter closed and the internal lamp power on. The external 200-Watt lamp is turned on to allow the lamp to warm up, but all radiation is blocked by the shutter.
- Item 2 measures PMT current between 250 and 334 nm with the 200-Watt lamp on and the shutter open. The integration time is 3 seconds per wavelength sampled.
- Item 3 measures PMT current between 335 and 700 nm with the 200-Watt lamp on and the shutter open. The integration time is 1 second.
- Item 4 measures PMT current between 250 and 700 nm with the 45-Watt lamp on and the shutter closed. The integration time is 1 second.
- Item 5 measures PMT dark current with the instrument's shutter closed and all lamps off.

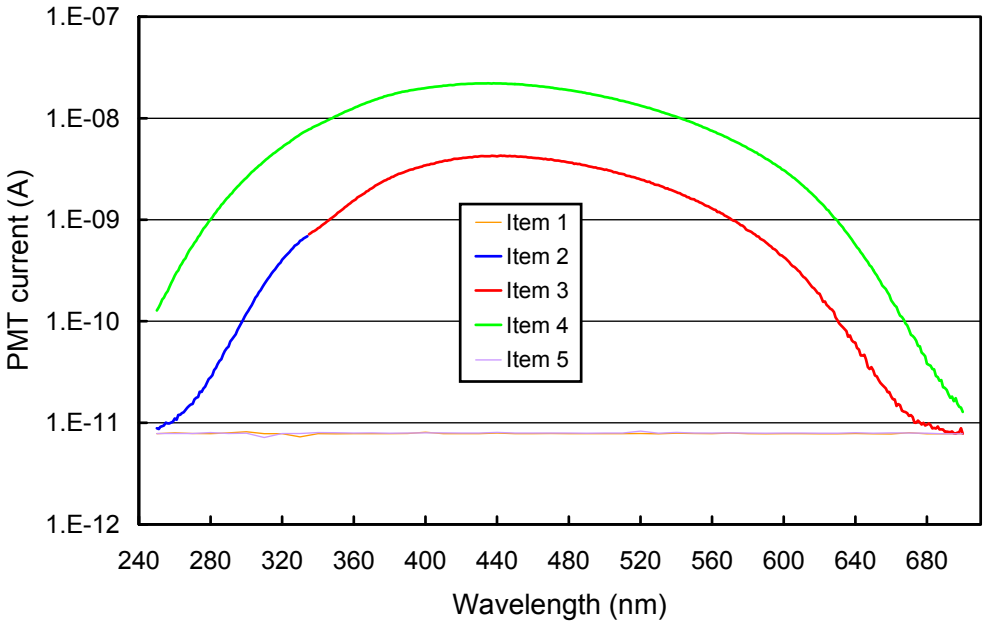

Figure 4.11. Typical five-item absolute scan of the SUV-150B spectroradiometer.

4.2. Calibration and Data Processing of SUV-100 and SUV-150B Data

This section describes the method used to calculate global spectral irradiance, biologically weighted dose-rates and daily doses from raw data generated by the spectroradiometers. The irradiance calibration of data scans is laid out in Section 4.2.1.; the wavelength calibration of the instruments is described in Section 4.2.2.

4.2.1. Irradiance Calibration

At each instrument site, an irradiance calibration ("absolute scan") is performed approximately bi-weekly. This section describes how:

- Values in calibration certificate of 200-Watt standards of spectral irradiance are interpolated (Section 4.2.1.1.)
- The internal irradiance reference lamp is calibrated (Section 4.2.1.2.)
- The system responsivity is determined, and solar data is calibrated (Section 4.2.1.3.)
- 200-Watt standards are intercompared (Section 4.2.1.4.)
- A calibration is transferred from one 200-Watt standard to a second one (Section 4.2.1.5.)

Most quantities used for these calculations are defined in Table 4.3.

Table 4.3 Notation of data processing parameters.

V	High voltage setting for the photomultiplier tube (PMT)
λ	Wavelength
$I_{dark}(V)$	Mean PMT dark current for a given PMT high voltage
$I_{ext}(\lambda,V)$	PMT current during a scan of an external 200-W standard of spectral irradiance
$I_{int}(\lambda,V)$	PMT current during a scan of the internal irradiance reference lamp
$I_{solar}(\lambda,V)$	PMT current during a solar data scan
$E_{interp}(\lambda)$	Interpolated irradiance values of a 200-Watt standard lamp, calculated from values provided in the lamp's certificate
$E_{int}(\lambda)$	Apparent irradiance of the internal irradiance reference lamp
$E_{solar}(\lambda)$	Solar irradiance
$R(\lambda,V)$	System responsivity

4.2.1.1. Interpolation of Values from Calibration Certificates of 200-Watt Standards

The irradiance calibration of the spectroradiometers is based on standards of spectral irradiance purchased from Optronic Laboratories. These are 200-Watt tungsten-halogen lamps of type Q6.6AT4/5CL manufactured by General Electric. Their calibration is traceable to the National Institute of Standards and Technology (NIST). The lamps are calibrated by Optronic Laboratories using an apparatus geometrically identical to that used at the sites, both in lamp orientation (downward light path) and lamp-to-collector

distance. To calibrate an SUV-100 spectroradiometer, one 200-Watt lamp is mounted every two weeks on top of the instrument and scanned (see Sections 2.5 and 4.1.5).

Standards of spectral irradiance are provided by Optronic Laboratories with a table of irradiance values in 10-nm increments. To calculate irradiance values in smaller wavelength increments for application at wavelengths obtained during the calibrations, a Black-Body function (or Planck equation) is used:

$$E_{\text{interp}}(\lambda) = a\frac{2hc^2}{\lambda^5}\frac{1}{\exp\{\frac{hc}{k\lambda T}\}-1}$$

where h is Planck's constant, c is the velocity of light, k is the Boltzmann constant, T is the temperature in Kelvin and $E_{\text{interp}}(\lambda)$ is the interpolated spectral irradiance. The term a is a scale factor. A least-squares fitting routine is used to adjust terms a and T for values provided from 290 to 600 nm (Figure 4.12).

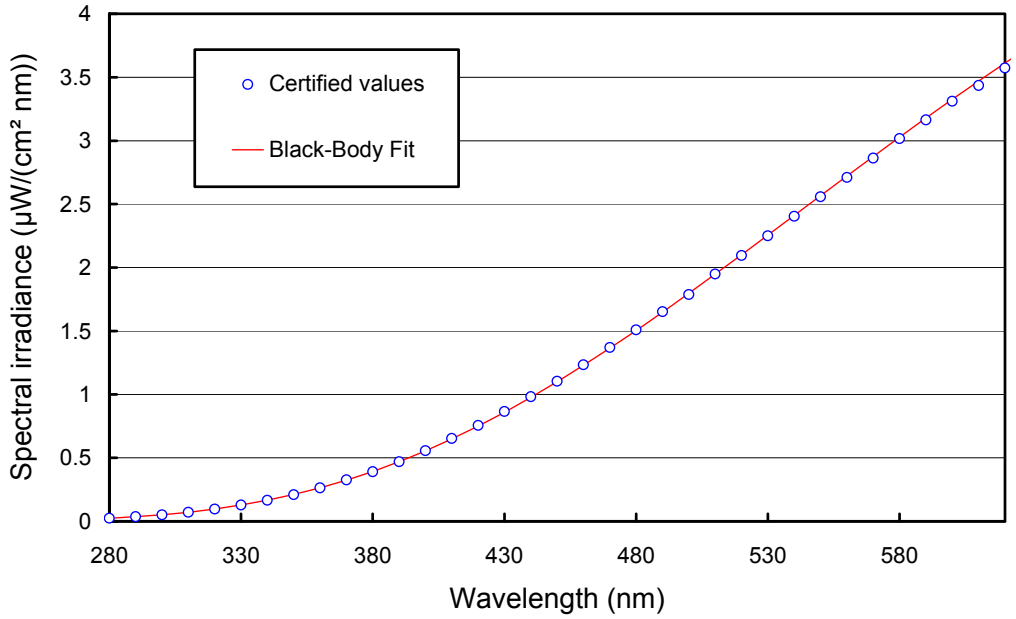

Figure 4.12. *Spectral irradiance of standard 200W010. The open circles are the values from the lamp's certificate provided by Optronic Laboratories. The red line is the Black-Body fit.*

Since a lamp spectrum is not a true Black-Body function, the fit will introduce an error. Figure 4.13 shows the ratio of the Black-Body fit values and the certified values of lamp 200W010. Both data sets agree to within ±1% for wavelengths above 290 nm, indicating that the error introduced by the fit is smaller than ±1%.

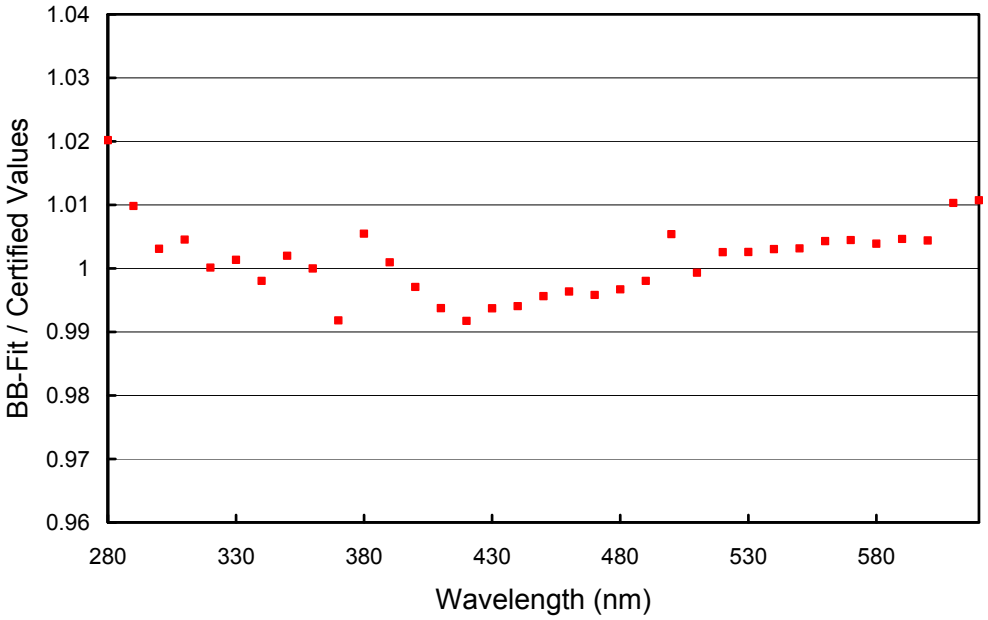

Figure 4.13. *Ratio of the Black-Body fit values and the certified values of lamp 200W010. Both data sets agree to within ±1%. The graph is based on the data shown in Figure 4.12.*

4.2.1.2. Calibration of the Internal Irradiance Reference Lamp

A system irradiance calibration is established by analyzing absolute scans (see Section 4.1.5). The procedure transfers the irradiance scale from the 200-Watt standard of spectral irradiance to the internal 45-Watt irradiance reference lamp. The irradiance $E_{\text{int}}(\lambda)$ assigned to the reference lamp is calculated with:

$$E_{\text{int}}(\lambda) = E_{\text{interp}}(\lambda)\frac{I_{\text{int}}(\lambda,V) - I_{\text{dark}}(V)}{I_{\text{ext}}(\lambda,V) - I_{\text{dark}}(V)},$$

where $I_{\text{int}}(\lambda,V)$ is the PMT current of the internal lamp measured during Items 3 and 7 (SUV-150B: Item 4) of an absolute scan. The PMT current when measuring the 200-W lamp, $I_{\text{ext}}(\lambda,V)$, is derived from Items 2 and 6 of the absolute scan (SUV-150B: Items 2 and 3). The PMT dark current $I_{\text{dark}}(V)$ is subtracted from both measurements. $E_{\text{interp}}(\lambda)$ is the interpolated irradiance of the 200-Watt lamp, calculated in the previous section. An absolute scan is usually preceded by a wavelength scan, which is used to correct the wavelength scale of the scan before the equation above is applied. Note that $E_{\text{int}}(\lambda)$ is not a "true" irradiance produced by the internal lamp at the place of the entrance optics but acts as a reference value when comparing the irradiance produced by the 200-Watt standard and solar irradiance.

Each bi-weekly calibration with a 200-Watt standard of spectral irradiance provides a function $E_{\text{int}}(\lambda)$. Ideally, these functions would not change from one calibration event to the next. In practice, there are changes due to:

- Drift of the internal lamp, i.e., the lamp became dimmer or brighter.
- Calibrations are performed with different 200-Watt standards.
- Random changes in the physical alignment of the 200-Watt standards, the supplied lamp current, or the lamp itself.

For these reasons, calibration of the spectroradiometer in a given time period is not based on one absolute scan only. An average irradiance $<E_{int}(\lambda)>$ of the internal lamp is calculated from *n* calibrations performed in time-intervals ranging from days to several months, depending on the stability of the internal lamp and other factors:

$$< E_{\text{int}}(\lambda) >= \frac{1}{n} \sum_{n} E_{\text{int},n}(\lambda)$$

In the following, $<E_{int}(\lambda)>$ is denoted "average-irradiance of the internal lamp." By this averaging, the influence of differences in the 200-W standards, and random errors, are reduced. If a response lamp drifts, the number of scans contributing to the average has to be limited. The allowed drift of the lamp is typically 2%. If the drift in any given period is larger, the period is broken in two or more parts with a separate average-irradiance value calculated for each part.

4.2.1.3. Determination of the System Responsivity and Calibration of Solar Data

The calculation of solar spectral irradiance at a particular time requires a data scan, a response scan, and a wavelength scan. Response and wavelength scans are typically taken from the same day as the data scan. In the first step, data and response scan are shifted with respect to wavelength based on the wavelength scan and a table, which defines non linearities in the monochromator's wavelength mapping. For Volumes 1- 6, this table was based on internal wavelength scans (Section 4.2.2.1); for later volumes, it is based on the Fraunhofer-correlation method described in Section 4.2.2.2. After all scans have been wavelength corrected, the responsivity *R* of the spectroradiometer is calculated:

$$R(\lambda, V) = \frac{I_{\text{int}}(\lambda, V) - I_{\text{dark}}(V)}{< E_{\text{int}}(\lambda) >}$$

Note that *R* is determined separately for each PMT high voltage setting. $I_{\text{dark}}(V)$ is calculated from the 280-290 nm portion of the data scan. The denominator $<E_{int}(\lambda)>$ is the response lamp's mean-irradiance, defined in the previous section.

The solar spectral irradiance, E_{solar}, is calculated from the PMT currents $I_{\text{solar}}(\lambda, V)$ of the data scan:

$$E_{\text{solar}}(\lambda) = \frac{I_{\text{solar}}(\lambda, V) - I_{\text{dark}}(V)}{R(\lambda, V)}$$

A typical solar irradiance spectrum created with this procedure has been shown in Figure 4.3.

4.2.1.4. Comparison of Standards of Spectral Irradiance

A solar irradiance spectrum calculated with the procedure above is only correct if (i) the irradiance scale preserved by the standards laboratory providing the lamp is correct, and (ii) the irradiance produced by the lamp when used at a given network site matches the values in the calibration certificate of the lamp. Systematic errors can stem from a variety of reasons, including:

- The 200-Watt lamp became dimmer or brighter since its calibration at the standards laboratory.
- The irradiance scale preserved by a given laboratory may change over time; i.e. standards purchased in different years may have different relative calibrations.
- Geometric errors; for example, the distance between lamp and fore-optics does not match the distance specified in the lamp's certificate.
- Thermal effects
- Operator errors

To verify the calibration of the irradiance standards used at the network sites, an engineer from Biospherical Instruments conducts a comparison of all on-site lamps with a "traveling" standard during the annual site visits. Based on these data, we determine if significant changes have occurred. From 2001 onward, each site is equipped with three standards (Historically, there were only two standards).

The comparison of 200-Watt lamps is based on the fact that spectral irradiance $E_{int}(\lambda)$, assigned to the internal lamp, should not depend on the 200-Watt lamp used for its calibration. Let us assume that the internal lamp is calibrated independently with two different 200-Watt standards, lamp #1 and #2. One standard is brighter than the other, and this difference is accurately indicated in the lamps' certificates. In this case, the brighter lamp will lead to a larger PMT current, $I_{ext}(\lambda)$. The irradiance assigned to the internal lamp, $E_{int}(\lambda)$, however, will not depend on the 200-W lamp used because the values in the calibration certificate are higher by the same amount. On the other hand, if there is a mismatch between the actual irradiance and the irradiance tabulated in the certificate of a 200-Watt lamp, $E_{int}(\lambda)$ will depend on the lamp used for the calibration. In more detail, the ratio $C(\lambda)$ between $E^{(1)}{}_{int}(\lambda)$, determined with lamp #1, and $E^{(2)}{}_{int}(\lambda)$, from lamp #2, allows us to quantify the difference between both calibration standards:

$$C(\lambda) = \frac{E_{\text{int}}^{(1)}(\lambda)}{E_{\text{int}}^{(2)}(\lambda)} = \frac{E_{\text{interp}}^{(1)}(\lambda)\dfrac{I_{\text{int}}^{(1)}(\lambda,V) - I_{\text{dark}}(V)}{I_{\text{ext}}^{(1)}(\lambda,V) - I_{\text{dark}}(V)}}{E_{\text{interp}}^{(2)}(\lambda)\dfrac{I_{\text{int}}^{(2)}(\lambda,V) - I_{\text{dark}}(V)}{I_{\text{ext}}^{(2)}(\lambda,V) - I_{\text{dark}}(V)}}$$

Only the definition of $E_{int}(\lambda)$, determined separately for lamp #1 and #2, was used in the above expression. If lamps #1 and #2 agreed with their certificates, $C(\lambda)$ would be 1. For the intercomparison to be valid, it is important that all scans are performed under the same conditions, i.e., the internal PMT currents $I_{\text{int}}^{(1)}(\lambda,V)$ and $I_{\text{int}}^{(2)}(\lambda,V)$ must be identical, i.e. the internal lamp is stable.

Figure 4.14 shows a comparison of the 200-Watt standards 200W010 (Lamp #1) and M-874 (Lamp #2). Both lamps were calibrated by Optronic Laboratories in September 1998. The comparison was performed on 9/3/97. In Figure 4.14, the function $C(\lambda) - 1$ is depicted. The curve should ideally be equal to the 0% line. In reality, the function deviates by approximately 5% in the UV and by 2% in the visible. Investigation revealed that lamp 200W010 had drifted over time, and that it was dimmer on 9/3/97 compared to September 1998, when it was (re)calibrated. A darkening of the lamp leads to a smaller $I_{\text{ext}}^{(1)}(\lambda,V)$. If $I_{\text{ext}}^{(1)}(\lambda,V)$ is low, $C(\lambda) - 1$ becomes larger than one, following the equation above. This is in agreement with the result presented in Figure 4.14. If the system had been calibrated with lamp 200W010 rather than M-874, solar irradiance measurements would be higher. Similar analyses from other sites and lamps are provided in Section 5.

A lamp drift of 5% within two years is unusually high. Normally, drifts of calibration standards are in the order of <2% per year. Some of the standards, which have been used during Volume 16, have two sets of calibration certificates, making it possible to track the drift of these lamps over time. See also Table 5.2 in the introduction to Section 5.

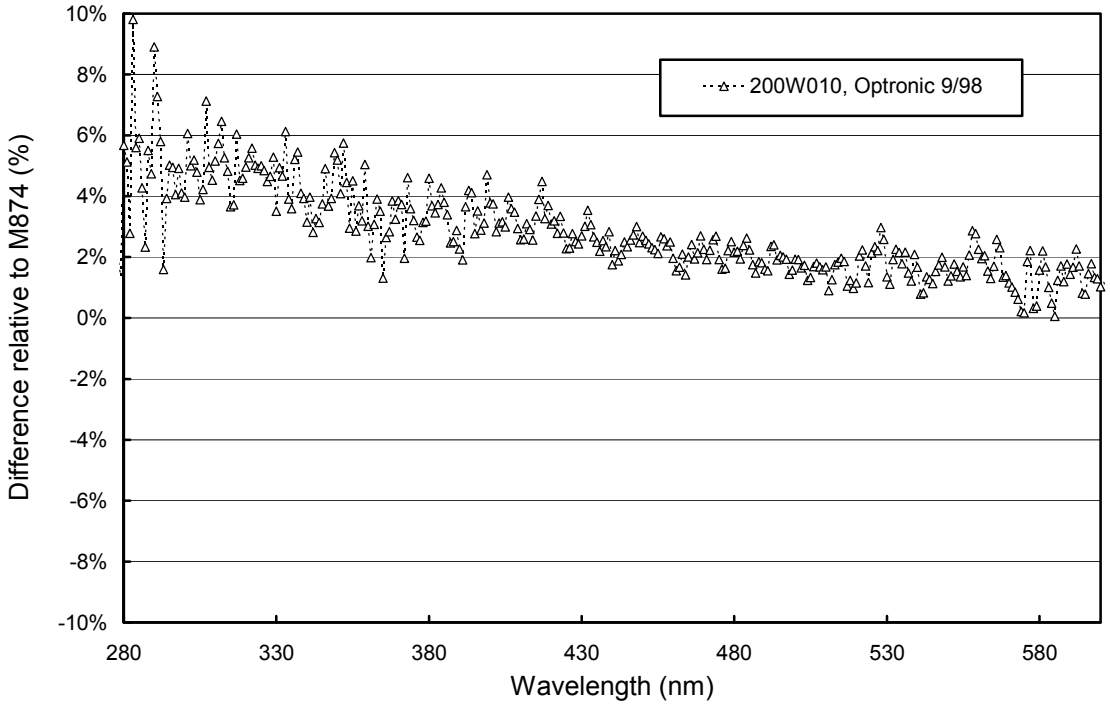

Figure 4.14. *Comparison of lamps 200W010 and M-874 expressed by the function C(λ) –1 . See text for details. The difference relative to M-874 is positive resulting in solar irradiance increasing if 200W010, rather than M-874, were used for calibration.*

4.2.1.5. Calibration of Lamps

Not all 200-Watt lamps used in the network have been calibrated by an independent standards laboratory. It is sometimes necessary to transfer a calibration from a calibrated "reference" lamp to other lamps. To calibrate a new lamp (or re-calibrate a lamp already in service), the new lamp and the reference lamp are operated consecutively, and spectral irradiance $E(\lambda)$ of the new lamp is calculated by:

$$E(\lambda) = E_{\mathrm{R}}(\lambda)\frac{I(\lambda,V) - I_{\mathrm{dark}}(V)}{I_{\mathrm{R}}(\lambda,V) - I_{\mathrm{dark}}(V)},$$

where $I_{\mathrm{R}}(\lambda,V)$ and $E_{\mathrm{R}}(\lambda)$ are PMT current and spectral irradiance of the reference lamp, respectively. Black-Body coefficients a and T are fitted to $E(\lambda)$ after completion of the calibration as outlined in Section 4.2.1.1. Note that the calibration procedure does not involve measurement of the internal 45-Watt lamp. Measurements of this lamp have historically been includes. See previous Operations Reports for details.

4.2.2. Wavelength Calibration and Correction

The wavelength calibration of Volumes 1 - 6 network data was solely based on internal mercury scans (Section 4.2.2.1). Starting with Volume 7, the method has been changed, see Section 4.2.2.2. The prior method is presented here because the results of internal mercury scans are also used in the new approach, although in a different way. Presentation of the original method gives some rational for the change implemented.

4.2.2.1. Wavelength Correction with Internal Mercury Scans Implemented for Volumes 1 - 6

The internal low-pressure mercury lamp produces a number of emission lines that are seen as high-intensity, narrow spikes in the wavelength scan (Figure 4.8). The wavelengths of these lines are fixed fundamentally and form the basis of the calibration. There are different methods for determining the location of a detected peak. Until 1994, the "FWHM-method" has been used; from 1994 until 2001, the "tangent" method has been applied. See previous Operations Reports for details. The latest data are calibrated with the "Gauss-fit method".

The Gauss-fit method fits a Gauss function of the type

$$z = a \times \exp[-b(\lambda - \lambda_c)^2]$$

to the data points of each spectral line that is part of the wavelength scan. The variables a and b are coefficients and λ_c is the center wavelength returned by the algorithm. In our implementation, the function is linearized, a is set to the measured maximum of the spectral line, and the coefficients b and λ_c are determined with a least-square fit.

The wavelength correction of data scans recorded in Volumes 1 - 6 was a two-step process. Step 1 takes account of the day-to-day wavelength fluctuations by aligning a spectrum to 296.73 nm, and Step 2 corrects for monochromator non-linearities that remain fairly constant throughout a season. In Step 1, the wavelength shift at the mercury line of 296.73 nm is determined from the daily automatic wavelength scans. By subtracting this wavelength from the true wavelength, 296.73 nm, the wavelength shift is determined. This shift is then applied to solar scans, i.e., the whole spectrum is shifted by a single constant value. In Step 2 of the procedure, a shift-function is applied that is calculated from 13 mercury lines of the wavelength scan. This function corrects for monochromator non-linearities. An example of this function is shown in Figure 4.15. The function is zero at 296.73 nm because it only describes wavelength deviations between measured and nominal wavelength positions relative to this wavelength. The function is usually very stable over a long period and is typically calculated from the average of all wavelength scans performed during the period of a data volume (or "season"). The function is described by a series of linear equations of the form $\Delta\lambda = a_n + b_n\lambda$ that are determined stepwise for peak-to-peak wavelength segments.

By examining all wavelength scans recorded during a season, ***three sources*** of uncertainty in the wavelength alignment appear.

First, there may be wavelength fluctuations within one day, which cannot be detected by wavelength scans that are usually performed only once a day. These variations can be attributed to power failures, loss of index in the stepping motor, thermal expansion of the monochromator due to temperature variations, other mechanical causes, and random noise in the peak-finding algorithm. Typically, the variation in the position of the 296.73-nm line is less than ±0.02 nm between consecutive wavelength scans and this value is therefore also a good estimate of the wavelength variation during one day. Figure 4.16 shows a typical distribution of the difference in the measured position of the 296.73 nm mercury line between consecutive wavelength scans.

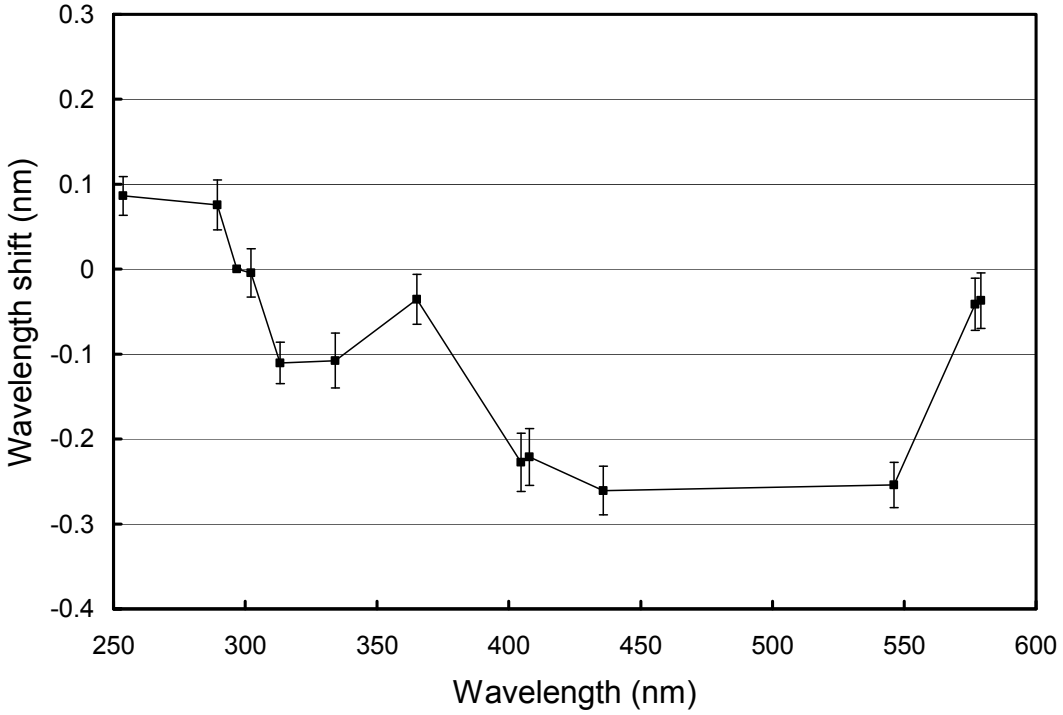

Figure 4.15. *Monochromator non-linearity correction function. Approximately 347 internal wavelength scans were evaluated. The error bars represent* $\pm 1\sigma$ *limits calculated from these scans.*

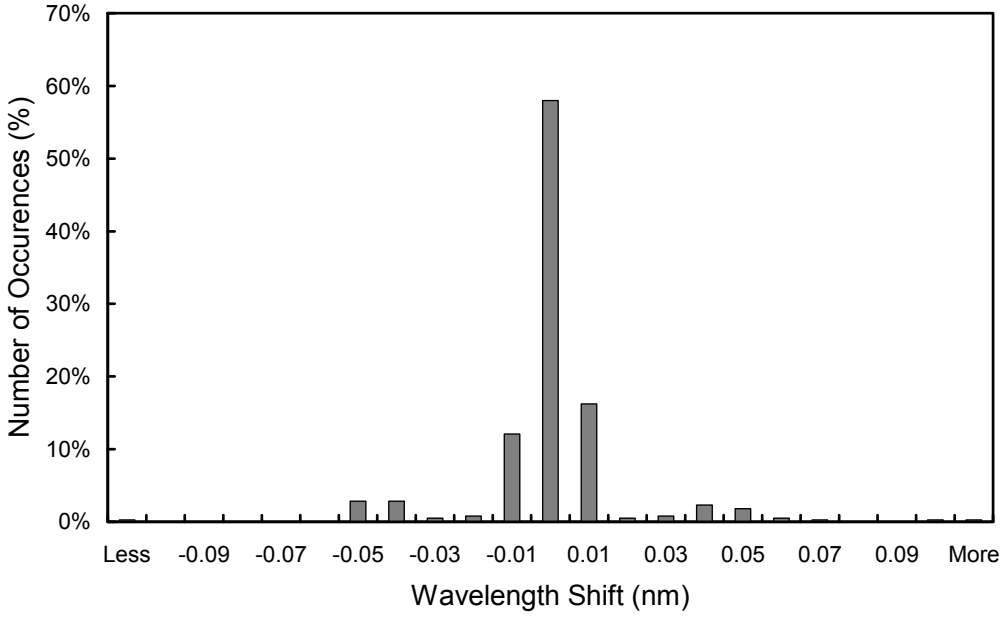

Figure 4.16. *Typical differences in the measured position of the 296.73 nm mercury line between consecutive wavelength scans.. The x-labels give the center wavelength shift for each column. Thus, the 0-nm histogram column covers the range -0.005 to +0.005 nm. "Less" means shifts smaller than –0.105 nm; "more" means shifts larger than 0.105 nm. For 88% of the days, the change in offset is smaller than ±0.025 nm.*

The **second** source of uncertainty is caused by changes in monochromator non-linearity during a season. Usually only one function is applied per season. The uncertainty caused by this approach is given by the standard deviation of the variation of individual wavelength scans. In the UV-B, the standard deviation (1σ) is often less than 0.02 nm, and increases to 0.05 nm in the visible. The uncertainty in the UV-B is lower because most of the fluctuations are removed by Step 1 described above.

A **third** source of error in the wavelength domain is caused by the different optical light paths for internal wavelength scans and measurements of solar irradiance. This effect can be tracked by comparing internal and external wavelength scans. The different geometry introduces a bias into the data that is usually constant throughout a season. Figure 4.17 indicates that the difference between both scan types may depend on wavelength. In this example, the difference at 296.73 nm is about 0.1 nm, increases to about 0.13 nm at 400 nm, and is about 0.05 nm in the visible. the wavelength dependence of the bias is different for every instrument. This bias has not been corrected in Volume 1 through 6 data. Starting with Volume 7, the problem has been addressed by implementing a method described in the next section.

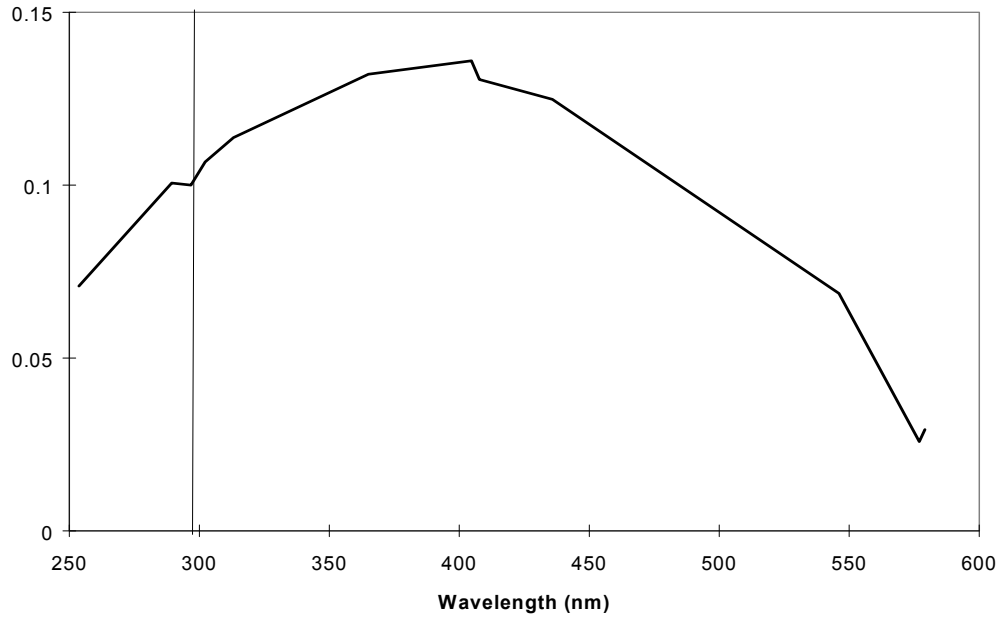

Figure 4.17. *Difference between the monochromator corrections based on external and internal mercury scans. The vertical line emphasizes the difference at 296.73 nm.*

4.2.2.2. Wavelength Calibration and Correction by the Fraunhofer-Correlation Method Implemented for Volume 7 – 16 Data

Principle of the correlation method

In order to improve the accuracy of the wavelength calibration and to avoid the problems associated with internal mercury scans, a different methodology has been implemented for Volumes 7 – 16. The method utilizes the Fraunhofer structure in solar spectra, which is caused by absorption processes in the Sun's outer atmosphere. This structure is also very marked in spectra of solar irradiance measured with the SUV-100 network radiometers, see for example Figure 4.3. By correlating the structure in measured spectra with a similar structure in a reference solar spectrum (i.e., a spectrum with negligible wavelength errors) the wavelength shift can be determined and the measured spectra corrected. Two different implementations of the correlation method were applied for Volume 16 data. One implementation is based on the method by Slaper et al. (1995), the other implementation is the method by Bernhard et al., 2004, which is also applied to Version 2 NSF network data (www.biospherical.com/nsf/Version2/). The method that was actually used for a given site is specified in Section 5, where quality control of each network site is discussed.

The correlation-software (SHICrivm Version 2.7.) for the method by Slaper et al. (1995) was provided by H. Slaper and extended to match data format and processing requirements of the NSF Network. The reference solar spectrum is based on a high-resolution (< 0.001 nm) extraterrestrial spectrum measured by the Fourier-Transform Spectroradiometer (FTS) at the National Solar Observatory (NSO) located at Kitt Peak, Arizona (Kurucz et al., 1984). The original spectrum was slightly modified by H. Slaper to account for an erroneous peak in the Kitt Peak spectrum in the 320-330 nm range (Slaper and Koskela, 1997). The wavelength accuracy of this spectrum has been proven to be better than 0.003 nm. The method has been successfully used to evaluate the results of several European intercomparison campaigns (Slaper et. al., 1995; Slaper, 1997; Slaper and Koskela, 1997; Reinen et. al., 1998; Seckmeyer et. al., 1998).

Implementation of the correlation method by Slaper et al. (1995)

The objective of the implementation is to define the monochromator non-linearity correction function. The set of linear functions presented in Section 4.2.1.1 is replaced by a set of similar functions derived from the Fraunhofer-correlation method.

The method can be used only in the wavelength range between 300 nm (310 nm for Barrow, McMurdo, and South Pole due to low solar elevations) and 440 nm. Below 300 nm, the signal is too noisy, i.e., the Fraunhofer structure in measured spectra is too distorted by noise to allow a reasonable correlation with the reference spectrum. Above 440 nm, the accuracy of the available reference spectrum is unknown and therefore we decided not to implement the method there.

In order to retrieve correction values outside the range of 300-440 nm we applied a combination of internal wavelength scans and the Fraunhofer-correlation method. In the first step, the mean deviation of wavelength shifts determined with internal wavelength scans and the Fraunhofer-correlation method is determined between 300 and 440 nm. For all sites the mean difference is typically between 0.08 and 0.15 nm. In a second step, the values of the internal wavelength scans outside the 300-440 nm range are shifted by this average value. We estimate the accuracy of this method for wavelengths in the critical region around 300 nm to be better than 0.05 nm. For example, the shift values for the two neighboring wavelengths 300 nm (Fraunhofer-based) and 296.73 nm (based on shifted internal wavelength scan) usually agree to within 0.03 nm. For wavelengths above 440 nm, the wavelength accuracy is less critical.

Figure 4.18 illustrates two functions expressing the monochromator non-linearity of the Barrow instrument during the Volume 7 season. The lower curve is based on the original method, i.e., only internal mercury scans have been evaluated. The upper curve was generated with the new Fraunhofer-correlation method. As described above, a pure Fraunhofer correlation was applied in the core range of 310-440 nm and the values outside this range are based on shifted internal scans. The difference between both curves is about 0.12 nm. The graph is based on data from the 1997-98 season and the upper curve represents the correction function that was actually applied to the Barrow data of this season.

In order to quantify the effect of the change in the wavelength correction method on solar irradiance data, a subset of San Diego Volume 7 data (9/9/97-12/31/97) was corrected with both the historic and the new procedures. Biologically effective UV dose-rates corrected with the old method are typically lower by 2-4% than dose-rates calculated with the Fraunhofer correlation method. Integrals in the UV-A and visible are virtually not affected by the change of the correction methods.

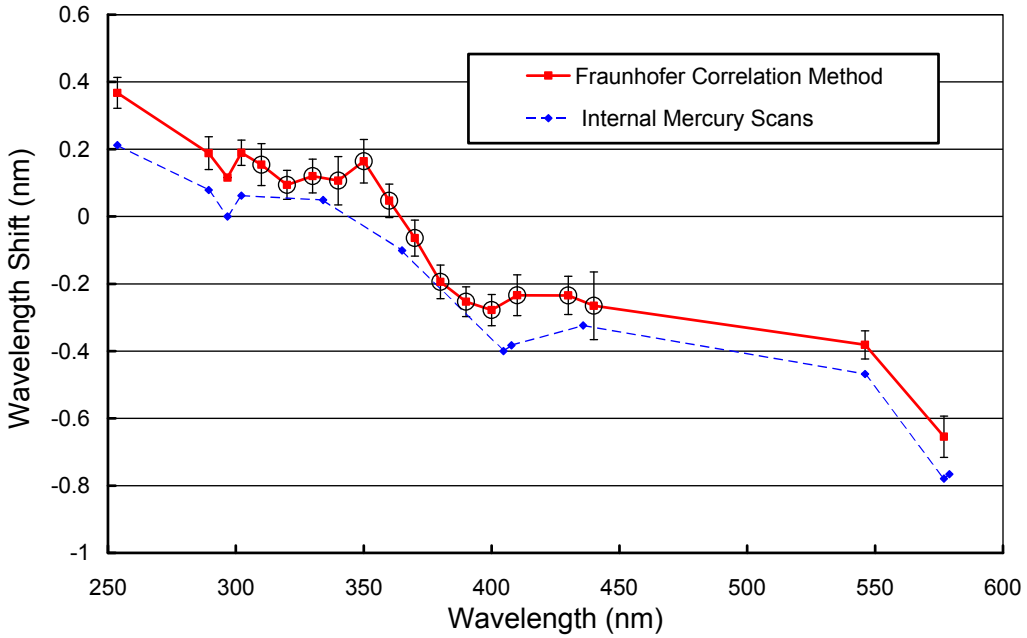

Figure 4.18. *Monochromator non-linearity correction function for Barrow Volume 7. Dashed blue line: Function calculated solely with internal mercury scans. Solid red line: Function calculated with a combination of results from the Fraunhofer-correlation method by Slaper et al. (1995) and internal mercury scans. Between 310 and 440 nm the function is based on the Fraunhofer-correlation method only (marked with circles in the plot). Outside this interval, the function is based on internal mercury scans, which were shifted by the mean difference between both methods. See text for a more detailed description. Both functions represent average wavelength shifts for the 1997-98 season. The error bars give the 2σ standard deviation variation of the wavelength shifts.*

Implementation of the correlation method by Bernhard et al. (2004a)

This method allows determination of the monochromator non-linearity correction function over the entire spectral range covered by data scans and does not require information from the internal wavelength scan. The measured spectrum is compared with a spectrum modeled with the radiative transfer model UVSPEC/libRadtran (Mayer and Kylling, 2005).

Differences between measurement and model that are not caused by wavelength shifts, may introduce errors into the shift analysis. It is therefore necessary to remove these differences before starting the correlation. In our implementation, we first apply smoothing to both the measured and modeled spectrum and correlate the ratio of original and smoothed measured spectrum against the ratio of original and smoothed model spectrum. The ratio of original and smoothed spectrum is typically very similar for the measured and modeled data sets, but both ratio-spectra are slightly shifted against each other. The correlation is performed by calculating the wavelength shift δ that leads to a minimum of the error ratio $E_R(\delta)$, defined as:

$$E_R(\delta) = \sqrt{\frac{\sum_{\lambda_m \in [\lambda_C - \lambda_I, \lambda_C + \lambda_I]} \left(\frac{r_M(\lambda_m)}{r_C(\lambda_m + \delta)} \right)^2}{m - 1}}$$

where λ_m are the discrete wavelengths of the measured spectrum

λ_C is wavelength for which the wavelength shift is calculated,

λ_I	is the half-width of the correlation interval,
δ	is the wavelength shift, given in multiples of 0.01 nm,
$r_M(\lambda)$	is the ratio of the original and smoothed measured spectrum,
$r_C(\lambda)$	is the ratio of the original and smoothed modeled spectrum given in steps of 0.01 nm, and
m	is the number of wavelengths λ_m in the interval $[\lambda_C - \lambda_I, \lambda_C + \lambda_I]$.

Measured spectra are corrected by adding the wavelength shift δ to the spectra's wavelength column. See Bernhard et al. (2004a) for more details on the method.

4.2.3. Biological Dose-Rate Calculations

The impact of radiation on biological systems is usually described as the integral of the product of spectral irradiance, *E(λ),* and a "biological weighting function" *W(λ)*:

$$E_{\text{bio}} = \int_{\lambda_1}^{\lambda_2} E(\lambda) W(\lambda)\, d\lambda$$

W(λ) is also often denoted "action spectrum" and is a dimensionless function. In this report, we refer to E_{bio} usually as a "biological dose-rate." (Integrating biological dose-rate over time results in a "biological dose", see Section 4.2.4). Spectral data from the UV network are routinely processed to calculate biological dose-rates according to several published weighting functions. The above integral is usually evaluated with the integration limits, 286 and 400 nm, respectively. The integration is approximated via a sum with $d\lambda = 0.2$ nm steps typically between 286 and 345 nm, and $d\lambda = 0.5$ nm steps between 345.0 and 400 nm, where applicable.

Published data include six biological dose-rates, abbreviated Setlow, Hunter, Caldwell, Dose1, Dose2, and Dose3_CIE_Erythema. The action spectra for these dose-rates are described below and are plotted in Figure 4.19 and Figure 4.20. The data of spectral irradiance were also weighted with the spectral responsivity of the TSI sensor (Figure 2.15) and also published. Please see the Appendix for a detailed listing of the code used to compute biological dose-rates from these weighting functions.

"Setlow" is based on a parameterization of the spectral dependence of damage to unprotected DNA that was suggested by R. B. Setlow (1974). The integration range is from 286 to 340 nm.

$$W(\lambda) = 10^{D(\lambda)}, \text{ where } D(\lambda) = \begin{cases} 13.04679 - 0.047012\lambda, 286 \le \lambda < 290 \\ 20.75595 - 0.073595\lambda, 290 \le \lambda < 295 \\ 30.12706 - 0.105362\lambda, 295 \le \lambda < 300 \\ 42.94028 - 0.148073\lambda, 300 \le \lambda < 305 \\ 45.24538 - 0.15563\lambda, 305 \le \lambda \le 340 \end{cases}$$

Please note that other parameterizations of Setlow (1974) exist. Care must be used when results of different implementations are compared.

"Hunter" is based on an exponential function fit to the data of J.H. Hunter, J.H. Taylor, and H.G. Moser (1979) and reported in numerical form by R.C. Smith and K. S. Baker (1982). The integration range is from 290 to 340 nm.

$$W(\lambda) = \exp\{61.1381 - 0.21551\lambda\}$$

"Caldwell" refers to a parameterization of A.E.S. Green, T. Sawada, and E.P. Shettle (1974) for Caldwell's data on the relative photon effectiveness of UV-B irradiation to induce biological response, when protein or nucleic acid chromophores are involved (M. M. Caldwell, 1971). Integration range is from 286 to 313 nm.

$$W(\lambda) = 2.618 \cdot (1 - (\frac{\lambda}{313.3})^2) \cdot \exp\{\frac{300 - \lambda}{31.08}\}$$

"Dose1" refers to an action spectrum of erythema defined by W.D. Komhyr and L. Machta (1973). The parameterization used is found in A.E.S. Green, T. Sawada, and E.P. Shettle (1974). The weighting function peaks at 296.5 nm. The integration range is 286 to 400 nm. Note that a coding error exists in data sets of Volumes 1-5 for this action spectrum.

$$W(\lambda) = \frac{0.04485}{1 + \exp[\frac{\lambda - 311.4}{3.13}]} + \frac{4 \cdot 0.9949 \cdot \exp[\frac{\lambda - 296.5}{2.692}]}{\{1 + \exp[\frac{\lambda - 296.5}{2.692}]\}^2}$$

"Dose2" refers to an alternative action spectrum for erythema in human skin proposed by B.L. Diffey (1987). It is a multisegment power fit to tabular data.

$$W(\lambda) = 10^{D(\lambda)}, \text{ where } D(\lambda) = \begin{cases} -1.215837 + 0.004728\lambda, 286 \le \lambda < 295 \\ 10.73862 - 0.035795\lambda, 295 \le \lambda < 300 \\ 17.54579 - 0.058486\lambda, 300 \le \lambda < 305 \\ 50.49061 - 0.166502\lambda, 305 \le \lambda < 310 \\ 27.87686 - 0.093554\lambda, 310 \le \lambda < 320 \\ 15.3893 - 0.054531\lambda, 320 \le \lambda < 335 \\ 1.703584 - 0.013555\lambda, 335 \le \lambda < 365 \\ 8.365825 - 0.031808\lambda, 365 \le \lambda < 380 \\ -1.705338 - 0.005305\lambda, 380 \le \lambda \le 400 \end{cases}$$

Please note that this function peaks at 295 nm.

"Dose3_CIE_Erythema" refers to the action spectrum for erythema in human skin proposed by McKinlay and Diffey (1987). This is the erythema action spectrum that is most widely used and it is often referred to as the "CIE action spectrum for erythema."

$$W(\lambda) = 10^{D(\lambda)}, \text{ where } D(\lambda) = \begin{cases} 0, & \text{for } 286 \le \lambda < 298 \\ -0.094(\lambda - 298), & \text{for } 298 \le \lambda < 328 \\ -0.015(\lambda - 139), & \text{for } 328 \le \lambda \le 400 \end{cases}$$

Note that this function equals "1" below 298 nm.

"Weighted TSI" is obtained by weighting spectral irradiance with the spectral responsivity of the TSI sensor. The sensor consists of a filtered photodiode. The responsivity function was calculated from spectral transmission of the filter and spectral response of the diode. The integration range is 320 to 392 nm and the function is parameterized as follows:

$$W(\lambda) = \begin{cases} 0.005598382 - 0.04901834\frac{\lambda}{1000} + 0.1420638(\frac{\lambda}{1000})^2 - 0.1361036(\frac{\lambda}{1000})^3, \lambda < 367 \\ -0.08228739 + 0.6492523\frac{\lambda}{1000} - 1.70513(\frac{\lambda}{1000})^2 + 1.490757(\frac{\lambda}{1000})^3, \lambda \ge 367 \end{cases}$$

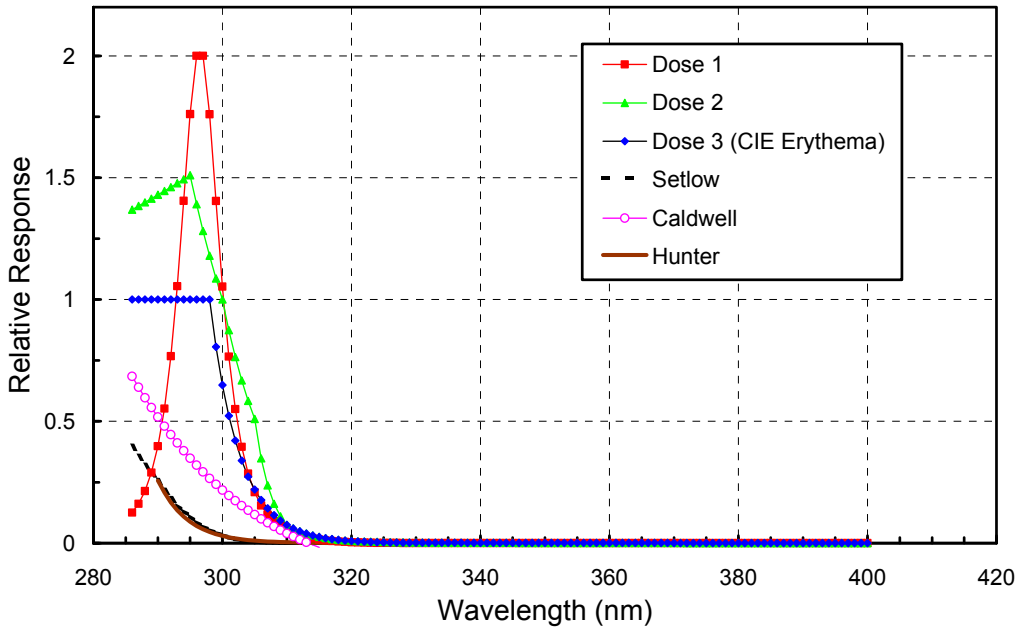

Figure 4.19. *Biological weighting functions used to calculate biological dose-rates from spectral irradiance data.*

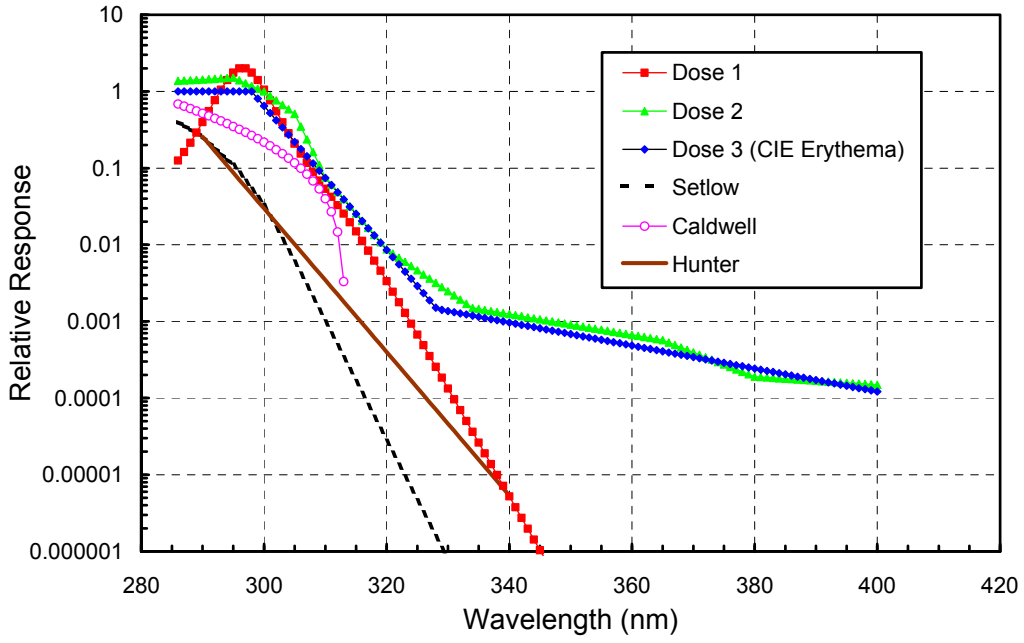

Figure 4.20. *Biological weighting functions as in Figure 4.19 but plotted on a logarithmic y-axis.*

4.2.4. Calculation of Daily Doses

Daily doses are calculated by integrating instantaneous irradiance values over time:

$$D = \int_{x-12}^{x+12} E(t)\,dt$$

Here *E* symbolizes either dose-rates or irradiance integrated over a specific wavelength range, for example spectral irradiance, integrated over 400-600 nm. The integration range is centered at approximate local noon *x* (01:00 UT for McMurdo, 16:00 UT for Palmer, 12:00 UT for South Pole, 17:00 UT for Ushuaia, 20:00 UT for San Diego, 22:00 UT for Barrow, and 15:00 for Summit). For example, the integration period for McMurdo is from 13:00 UT of the preceding day until 13:00 UT of the current day.

The integration is affected by gaps in the data and the fact that the first and last measurement of a given day usually occur during times when light levels are already significantly above zero. Therefore, interpolation and extrapolation of the measured data set is necessary before the integration can be performed. This is done by fitting a spline curve through the measured data points. The procedure is explained with Figure 4.21.

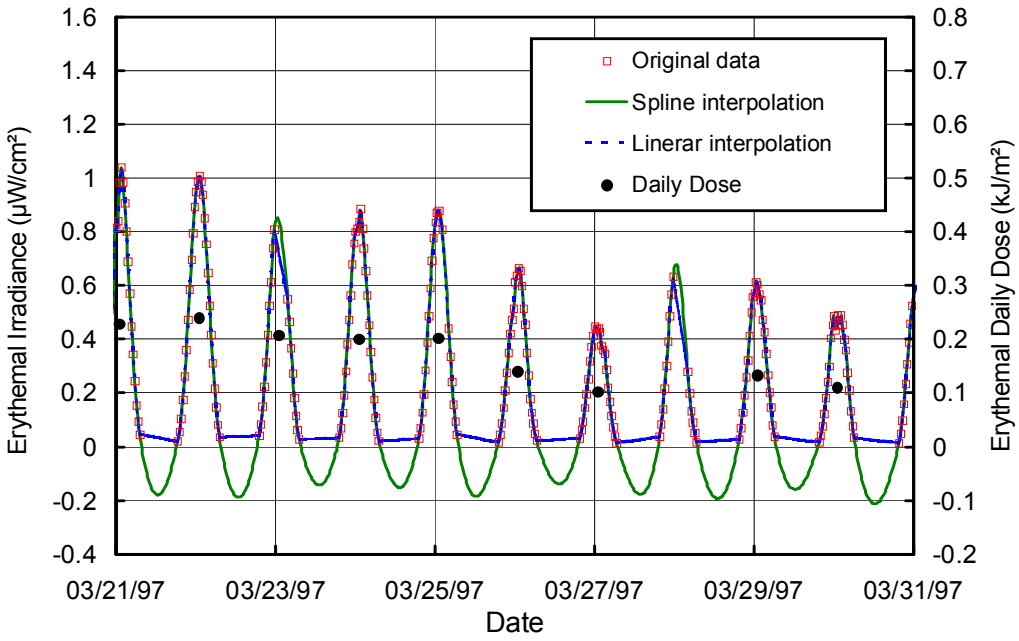

Figure 4.21. *Explanation of procedure to calculate daily doses. Squares: Measured erythemally weighted irradiance (left axis). Solid line: Spline interpolation of measured data. Broken line: Linear interpolation. Filled circles: Calculated erythemal daily dose (right axis).*

It can be seen from Figure 4.21 that the spline-interpolated curve fills gaps in measured data in a reasonable fashion. In particular when measurements are missing around noon-time (e.g. 3/23/97 and 3/28/97), spline-interpolation is superior to linear interpolation. When the spline-curve is negative, values are set to zero. The calculated daily dose is proportional to the area limited by the zero-line and the spline-curve. When gaps in data are too large, the calculation of daily doses is clearly not appropriate. The time limit is set to 15000 seconds. Daily doses for days with larger gaps (such as 3/28/97) are not included in published data.

4.2.5. Calculation of Solar Zenith and Azimuth Angles

All data in the databases on CD-ROM are accompanied with solar zenith and azimuth angles at the middle of a data scan. Both angles were calculated according to an algorithm presented by Wilson (1980).

4.3. Processing of Data from GUV Multichannel Radiometers

Data from GUV-511 and GUV-541 multichannel radiometers are tied to the SUV spectroradiometer located at the same site as the GUV to be calibrated. Final GUV data are prepared only after quality control of data from the collocated SUV has been complete. The methods for the calibration of GUV instruments and the calculation of GUV data products are based on algorithms developed by Dahlback (1996). More details on the procedure, including a validation of data products derived from NSF network GUV instruments, has been described by Bernhard et al. (2005b).

4.3.1. Calibration of GUV Radiometers

4.3.1.1. Calibration of GUV UV Channels

For each GUV UV channel *i*, a calibration factor k_i is determined according to the method originally proposed by Dahlback (1996):

$$k_i = \frac{V_i - O_i}{\int_0^\infty R_{D,i}(\lambda)\ \ E(\lambda)\ \ d\lambda} = \frac{V_i - O_i}{W_i}, \qquad \text{(G1)}$$

where
- $E(\lambda)$ is spectral irradiance at the plane of the GUV's collector,
- V_i is the signal of GUV channel *i*,
- O_i is the offset of GUV channel *i*,
- $R_{D,i}(\lambda)$ is the spectral response of channel *i*, and
- W_i is spectral irradiance weighted with the spectral response of channel *i*.

The PAR channel of GUV-511 radiometers is treated differently, see Section 4.3.1.2.

Offsets O_i are determined from night-time measurements. During periods of 24 hours of daylight, offsets are measured every two weeks by covering the GUV collector. Spectral response functions $R_{D,i}(\lambda)$ of all GUV UV channels were measured in the laboratory of Biospherical Instruments with a test apparatus specifically built for this purpose. Details on this apparatus and the measurement procedure were described by Bernhard et al. (2005b).

Spectral irradiance $E(\lambda)$ is based on measurements of the SUV spectroradiometer collocated with the GUV instrument. Calibration factors k_i are determined by correlating net-signals ($V_i - O_i$) of the GUV [numerator of Eq. (G1)] against W_i, typically using all SUV measurements from a complete data volume. To minimize errors due to the different sampling rates of GUV and SUV, GUV minute-by-minute measurements of channel *i* are interpolated to the times when the SUV measures at the nominal wavelength of channel *i*. Two different SUV data sets are considered for the calibration:

1. SUV data processed according to the method outlined in Section 4.2. These data have not been corrected for the cosine error of SUV spectroradiometers. GUV data based on this data set are

labeled with the suffix "U" in published GUV databases (see Section 6). This data set is best suited for comparisons with "Version 0" SUV-data described in this report.

2. Cosine corrected SUV data. The cosine correction schema is based on a method described by Seckmeyer and Bernhard (1993) and assumes clear sky conditions. The cosine correction factor $f_{G,i}(\theta,\lambda_i)$ for channel *i* is:

$$f_{G,i}(\theta,\lambda_i) = f_B(\theta,\lambda_i)\ \ R(\theta,\lambda_i) + f_D(\lambda_i)\ \ [1 - R(\theta,\lambda_i)], \qquad \text{(G2)}$$

where θ is solar zenith angle (SZA),

λ_i is nominal wavelength of channel *i*,

$f_B(\theta,\lambda_i)$ is the cosine error of the SUV, defined as the ratio of measured to true irradiance from the Sun's direct beam on a horizontal surface,

$f_D(\lambda_i)$ is the diffuse cosine error of the SUV, defined as the error in measuring isotropic radiance originating from the upper hemisphere: $f_D(\lambda_i) = \dfrac{\int_{(2\pi)} f_B(\theta,\lambda_i)\ \ \cos(\theta)\ \ d\Omega}{\int_{(2\pi)} \cos(\theta)\ \ d\Omega}$, where Ω is solid angle, and

$R(\theta,\lambda_i)$ is the ratio of beam irradiance on a horizontal surface, $E_B(\theta,\lambda_i)$, and global irradiance $E_G(\theta,\lambda_i)$: $R(\theta,\lambda_i) = E_B(\theta,\lambda_i)/E_G(\theta,\lambda_i)$.

$R(\theta,\lambda)$ is estimated with the radiative transfer model UVSPEC/libRadtran (Mayer and Kylling, 2005b). SUV data are cosine corrected by dividing the uncorrected data set with $f_G(\theta,\lambda)$. This corrected data set is then used for the correlation with GUV data to calculate calibration factors k_i. GUV data calibrated this way are labeled with the suffix "C" in published databases (see Section 6). The "C" dataset is more accurate than the "U" data set and typically 5% higher. This data set should also be used for comparisons with "Version 2" SUV data of NSF UV Monitoring Network (Bernhard et al., 2004).

Figure 4.22 shows a comparison of SUV measurements and calibrated GUV-511 measurements performed at San Diego between August 2003 and October 2004. GUV-511 measurements were calibrated against cosine-corrected SUV data. At small SZAs, good agreement of the two data sets can be expected due to the way the calibration is established. For the GUV 305 channel, both data sets agree on average to within ±5% for SZAs up to 75°. Between SZAs of 75° and 85°, the GUV data are systematically smaller than SUV measurements. This bias is likely due to a mismatch of the actual and measured response function $R_{D,305}(\lambda)$ of the GUV's 305 nm channel. Due to the large change of the solar spectrum in the UV-B, even small errors in the measurement of the function can have a pronounced effect (Bernhard et al., 2005b). For SZAs larger than 85°, radiation levels are very small and GUV measurements are close to the detection limit. This explains the large scatter in the ratio of GUV and SUV measurements at large SZAs. Calibrated measurements of the GUV's 340 nm channel agree with SUV data on average to within ±2% for SZA up to 93°. This wavelength is not affected by ozone absorption and measurements of the GUV are well above the detection limit even if the Sun is already below the horizon.

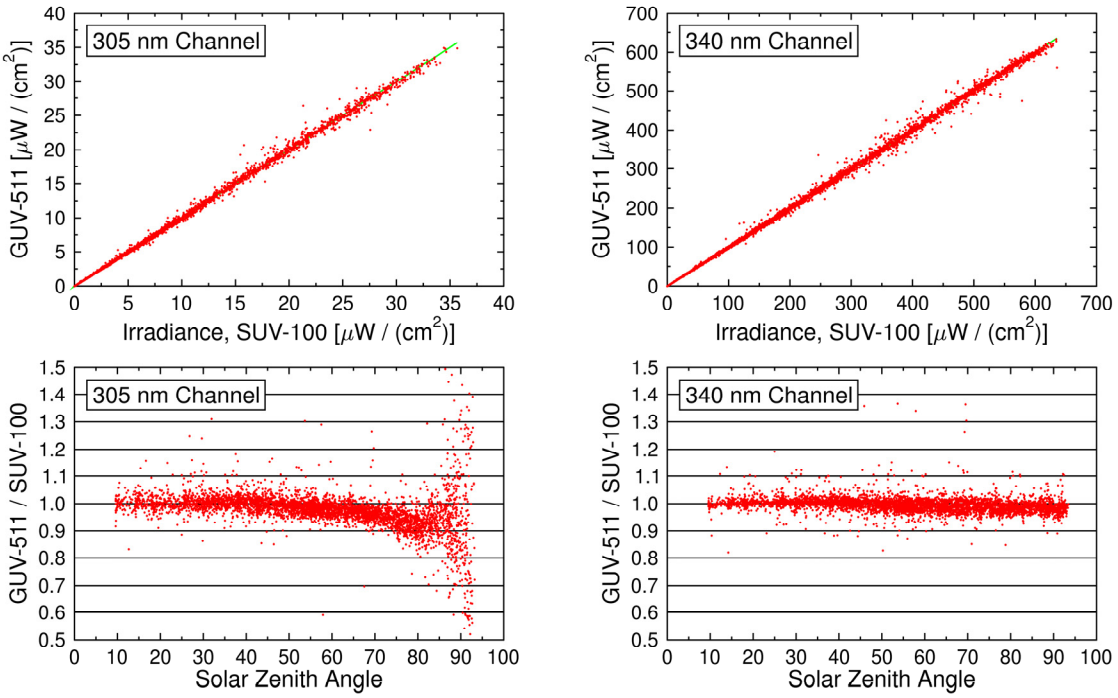

Figure 4.22. *Comparison of SUV-100 calibrated GUV-511 (S/N 9298) measurements at San Diego. Data is from the period August 2003 – October 2004. GUV-511 measurements were calibrated with cosine-corrected SUV-100 data. Top left: correlation of GUV and SUV measurements at 305 nm. Top right: correlation of GUV and SUV measurements at 340 nm. Bottom left: ratio of GUV and SUV measurements at 305 nm. Bottom right: ratio of GUV and SUV measurements at 340 nm.*

4.3.1.2. Calibration of GUV PAR Channel

Photosynthetically Active Radiation (PAR) is defined as radiation with wavelengths between 400 and 700 nm. The PAR channel of the GUV-511 radiometer measures photosynthetic photon flux density (PPFD), defined as number of photons in the 400-700 nm wavelength interval incident per unit time on a unit surface. The energy of a photon with wavelength λ is $h\nu = hc/\lambda$, where h is the Planck constant ($h = 6.626\text{x}10^{-34}$ Js), ν is the photon's frequency, and c is the speed of light ($c = 2.998\text{x}10^{8}$ m/s). Using this conversion, *PPFD* can readily be calculated from spectral irradiance $E(\lambda)$:

$$PPFD = \int_{400\ \text{nm}}^{700\ \text{nm}} E(\lambda)\frac{\lambda}{hc}d\lambda \qquad \text{(G3)}$$

PPFD is reported in units of μE/(cm^2 s). ("E" stands for Einstein. 1 E equals 1 mol of photons or $6.022\text{x}10^{23}$ photons.)

If SUV instruments were measuring up to 700 nm, *PPFD* cloud be calculated from SUV spectra with Eq. (G3) and compared with GUV measurements to calculate a calibration factor k_{PAR} in the same way UV channels are treated. Since SUV spectra terminate at 600 nm, a different method to calculate *PPFD* was chosen. Specifically, we use the following parameterization to estimate *PPFD*:

$$PPFD_{\text{estimated}} = c_1 E(400\text{nm}) + c_2 E(500\text{nm}) + c_3 E(600\text{nm}), \qquad \text{(G4)}$$

where E(400nm), E(500nm), and E(600nm) are spectral irradiance measured by the SUV at 400, 500, and 600 nm. The coefficients c_1, c_2, and c_3 are:

$$c_1 = -0.000156483 \text{ (µE nm)/(µW s)}$$
$$c_2 = 0.00134676 \text{ (µE nm)/(µW s)}$$
$$c_3 = 5.52304\ 10^{-5} \text{ (µE nm)/(µW s).}$$

The values of the three coefficients were determined from model spectra calculated for wavelengths up to 700 nm. Spectra were modeled for clear-sky conditions, sea level, and surface albedo of 7%. From these spectra, *PPFD* was calculated with Eq. (G3) and the coefficients were determined with a similar inversion method as described in Section 4.3.2. By using different sets of model spectra, is was confirmed that the same set of coefficients can also be applied for conditions with high surface albedo. *PPFD* and $PPFD_{\text{estimated}}$ agree with each other to within ±1% for SZAs between 0° and 85° and surface albedo between 0% and 97%. Systematic differences between exact calculation and parameterization may be higher during heavy-cloud conditions due to some water absorptions lines between 600 and 700 nm.

The calibration factor k_{PAR} is finally calculated with the method described in Section 4.3.1.1 using $PPFD_{\text{estimated}}$ for the correlation.

Prior to deployment of all GUV instruments, GUV PAR channels were also calibrated in the Biospherical Instruments laboratory using NIST traceable 1000-W calibration standards. Lab-based calibration factors agree to within ±5% with calibration factors calculated from SUV measurements. This level of agreement is within the combined uncertainty of both calibration methods. To avoid data loss, network GUV instruments are not regularly returned to Biospherical Instruments for re-calibration. The instruments are annually compared with SUV measurements for analyzing instrument drifts and adjustment of calibration factors.

4.3.2. Calculation of Integrals and Dose Rates from GUV Measurements

The conversion from "response-function-weighted irradiance" W_i to useful data products D, such as erythemal irradiance, is performed with the method suggested by Dahlback (1996). In brief, D is approximated by a linear combination of the net-signals from the GUV UV channels:

$$D = \sum_i a_i (V_i - O_i) \tag{G4}$$

The coefficients a_i are calculated by solving the system of linear equations:

$$\sum_i \left(a_i k_i \int_0^\infty R_{D,i}(\lambda)\ \ E_{M_j}(\lambda)\ \ d\lambda \right) = \int_0^\infty A(\lambda)\ \ E_{M_j}(\lambda)\ \ d\lambda\,, \tag{G5}$$

where $A(\lambda)$ is the action spectrum of the biological effect under consideration, and $E_{M_j}(\lambda)$ are model spectra calculated for different SZAs and ozone columns. These spectra are required to quantify the relative spectral difference between the GUV response functions and the action spectrum. For this study, model spectra were calculated with the radiative transfer model UVSPEC/libRadtran (Mayer and Kylling, 2005b). The values of the coefficients a_i determined with this method are not very sensitive to the set of model spectra used. However, for the most accurate results, model input parameters such as surface albedo and altitude were chosen to match the prevailing conditions at the deployment site of the GUV under test. The number of channels i, may range between 1 and 5, depending on the action spectrum used, and the number of model spectra required for the inversion has to match this number. For example, to calculate the set of coefficients a_i for the erythema action spectrum for a GUV deployed at San Diego, we used all four GUV-511 UV channels, and four model spectra calculated for combinations of SZA and total ozone of 30°, 250DU; 30°, 400DU; 70°, 250DU; and 70°, 400DU.

We are calculating 15 different wavelength integrals and 15 different dose-rates from GUV data with the method outlined above. Table 4.4 gives an overview of the wavelength bands and action spectra implemented. Numerical data of action spectra are available at www.biospherical.com/nsf/login/GUV/description-GUV-data-products.html or by request.

Table 4.4. GUV data products

Spectral irradiance:[a]
305 nm, 320 nm, 340 nm, 380 nm, 400 nm, 500 nm, and 600 nm

Integrals:[b]
290–315 nm, 290–320 nm, 315–360 nm, 320–360 nm, 360–400 nm, 315–400 nm, 320–400nm, and 400–600 nm

Dose-rates:

Effect	References	Remarks
Erythema	*McKinlay and Diffey (1987), Komhyr and Machta (1973), Diffey (1987), Anders et al. (1995)*	Four different action spectra are implemented.
UV Index	*McKinlay and Diffey (1987), WMO (1998)*	
DNA damage	*Setlow (1974)*	Four parameterizations of the action spectrum are implemented.
Skin cancer in mice	*Gruijl et al. (1993)*	Often referred to as SCUP-m
Skin cancer in mice corrected for human skin	*Gruijl et al. (1993)*	Often referred to as SCUP-h
Generalized plant damage	*Caldwell (1971)*	
Plant growth	*Flint and Caldwell (2003)*	
Damage to anchovy	*Hunter et al. (1979)*	
Inhibition of phytoplankton carbon fixation	*Boucher and Prezelin (1996)*	
Inhibition of phytoplankton photosynthesis of phaeodactylum and prorocentrum	*Cullen et al. (1992)*	
Inhibition of photosynthesis in Antarctic phytoplankton	*Neale and Kieber (2000)*	

Additional:
Spectral irradiance weighted with the response of several broadband filter radiometers, Photosynthetically Active Radiation (PAR), total column ozone.

[a] The "action spectra" for the calculation of spectral irradiances are triangular functions with a bandwidth of 1 nm FWHM centered at the specified wavelengths.

[b] The "action spectra" for the calculation of integrals are rectangular functions set to one within the specified interval and to zero outside this interval.

A comprehensive validation of the conversion method can be found in the paper by Bernhard et al. (2005b). As an example, Figure 4.23 shows a comparison of GUV and SUV-100 results for four data products: the UV Index (WMO, 1998), DNA-damaging radiation (Setlow, 1974), generalized plant damage (Caldwell, 1971), and UV-A. The data were measured at San Diego between July 20 and July 24, 2003. "Day 1" was cloudless, "Day 2" had variable cloud cover, and "Day 3" was overcast (see Figure 4.23 for "Day" assignment). UV-Index and UV-A measurements of the two instruments agreed to within ±10% (maximum deviation) for all three days, when SZA was smaller than 80°. The agreement for the DNA- and plant-damage data sets are similar when the data sets are filtered for SZAs smaller than 70°. At larger SZAs (when absolute values are very small), relative differences can be substantial. The agreement is generally better for data products that are not (or only slightly) sensitive to atmospheric ozone concentration. The scatter in the ratio of both instruments is somewhat larger during cloudy periods, which is due to the different sampling schemes of the two instruments. The GUV reports one-minute averages,

whereas the SUV requires several minutes to scan between 290 and 400 nm. Radiation levels may change during this period. Differences in the cosine errors of the two instruments cause the diurnal variation in the ratio for UV-A on Day 1 (Panel D). In contrast, there is little variation on the overcast Day 3, when the radiation field was more isotropic.

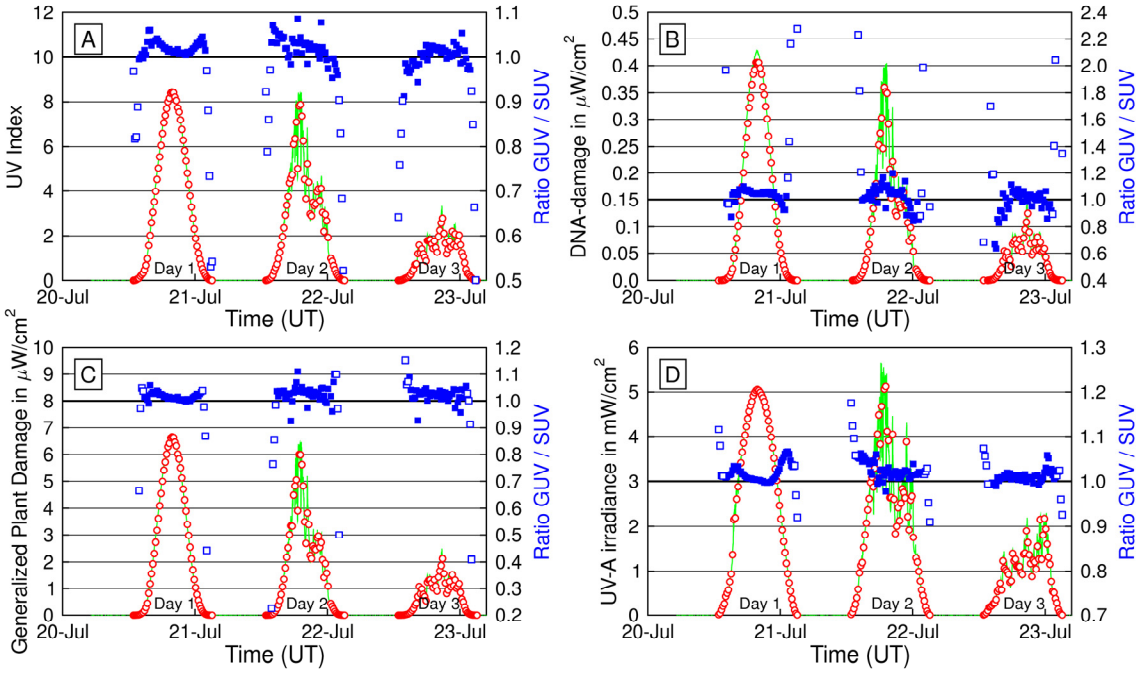

Figure 4.23. *Comparison of four different data products measured by GUV S/N 9298 (green line, left axis) and SUV-100 (open red circles, left axis) at San Diego between July 20 and July 24, 2003. GUV data are one-minute averages, SUV data were calculated from spectra measured every 15 minutes. Panel A: UV Index. Panel B: DNA-damaging radiation. Panel C: Generalized plant damage. Panel D: UV-A (320-400 nm). For Panels A and D, solid (open) blue squares indicate the ratios of GUV and SUV measurements for SZA <80° (>80°). For Panel B and C, solid (open) blue squares indicate the ratio GUV/SUV for SZA <70° (>70°).*

4.3.3 Calculation of Total Column Ozone from GUV Measurements

Total ozone column is calculated from GUV measurements with lookup tables, which relate total column ozone to SZA and the ratio of GUV measurements at 305 and 340 nm. The retrieval algorithm is similar to the method described by Stamnes et al. (1991). Lookup tables are calculated with the radiative transfer model UVSPEC/libRadtran, and resulting model spectra are weighted with the GUV response functions at 305 and 340 nm. Separate look-up tables are calculated for each site, taking into account site-specific conditions such as altitude, albedo, ozone profile, etc. On average, GUV total ozone data agree with TOMS data to within ±5% for SZA smaller than 75°. At larger SZA, differences become greater due to the dependence of the retrieval on the vertical distribution of ozone in the atmosphere. Also noise in the GUV's 305 channel affects the ability to calculate total ozone with good precision at large SZAs. A systematic comparison of GUV and TOMS total ozone measurements at several sites was performed by Bernhard et al. (2005b).